REPORT DOCUMENTATION PAGE

Form Approved
OMB No. 0704-0188

1. REPORT DATE *(DD-MM-YYYY)*	2. REPORT TYPE	3. DATES COVERED *(From - To)*
11-12-2008	Journal Article	

4. TITLE AND SUBTITLE

Non-Porous Organic Solids Capable of Dynamically Resolving Mixtures of Diiodoperfluoroalkanes (Preprint)

5a. CONTRACT NUMBER

5b. GRANT NUMBER

5c. PROGRAM ELEMENT NUMBER

6. AUTHOR(S)
P. Metrangolo, Y. Carcenac, & G. Resnati (Politecnico di Milano Univ., Italy); M. Lahtinen & K. Rissanen (Univ. of Jyväskylä, Finland); T. Pilati (Univ. of Milan); A. Vij (AFRL/RZSP)

5d. PROJECT NUMBER

5e. TASK NUMBER

5f. WORK UNIT NUMBER
50260541

7. PERFORMING ORGANIZATION NAME(S) AND ADDRESS(ES)

Air Force Research Laboratory (AFMC)
AFRL/RZSP
10 E. Saturn Blvd.
Edwards AFB CA 93524-7680

8. PERFORMING ORGANIZATION REPORT NUMBER

AFRL-RZ-ED-JA-2008-596

9. SPONSORING / MONITORING AGENCY NAME(S) AND ADDRESS(ES)

Air Force Research Laboratory (AFMC)
AFRL/RZS
5 Pollux Drive
Edwards AFB CA 93524-7048

10. SPONSOR/MONITOR'S ACRONYM(S)

11. SPONSOR/MONITOR'S NUMBER(S)
AFRL-RZ-ED-JA-2008-596

12. DISTRIBUTION / AVAILABILITY STATEMENT

Approved for public release; distribution unlimited (PA #09007).

13. SUPPLEMENTARY NOTES
For publication in Science Magazine.

14. ABSTRACT

A well-known class of organic non-porous compounds, polymethylene bismethonium iodides, undergoes selective capture and release of a,w-diiodoperfluoroalkanes in a dynamic and controlled manner, in solution and from the gas phase. Despite a lack of porosity of the starting materials, guest transport through the solid occurs readily until a thermodynamically stable porous structure is achieved, which is highly selective only to the convenient diiodoperfluoroalkane. The size matching between the inter-charge distance in the cation and the charge separation in the halogen-bonded I-···I(CF2)mI···I- superanion drives the selectivity of the process, which identifies the target diiodoperfluoroalkane even from complex industrial mixtures. The full reversibility of the process where diiodoperfluoroalkanes can first be selectively complexed and then quantitatively evacuated, yields pure fluorinated telomers and reusable decamethonium congeners.

15. SUBJECT TERMS

16. SECURITY CLASSIFICATION OF:			17. LIMITATION OF ABSTRACT	18. NUMBER OF PAGES	19a. NAME OF RESPONSIBLE PERSON
					Dr. Ashwani Vij
a. REPORT	b. ABSTRACT	c. THIS PAGE	SAR	63	19b. TELEPHONE NUMBER *(include area code)*
Unclassified	**Unclassified**	**Unclassified**			N/A

Standard Form 298 (Rev. 8-98)
Prescribed by ANSI Std. 239.18

Non-Porous Organic Solids Capable of Dynamically Resolving Mixtures of Diiodoperfluoroalkanes (Preprint)

Pierangelo Metrangolo,[1]* Yvan Carcenac,[1] Manu Lahtinen,[2] Tullio Pilati,[3] Kari Rissanen,[4] Ashwani Vij,[5] Giuseppe Resnati[1,3]

[1] NFMLab — DCMIC ''G. Natta'', Politecnico di Milano, via L. Mancinelli 7, 20131, Milan, Italy; Tel.: +39 02 2399 3041 (PM), 3032 (GR); Fax: +39 02 2399 3180; Web-site: http://nfmlab.chem.polimi.it. [2] Department of Chemistry, University of Jyväskylä, P.O. Box 35, Jyväskylä, FI–40014, Finland. [3] ISTM-CNR, University of Milan, 20133, Milan, Italy. [4] Nanoscience Center, Department of Chemistry, University of Jyväskylä, P.O. Box 35, Jyväskylä, FI–40014, Finland. [5] Space and Missile Propulsion Division, Air Force Research Laboratory, 10 E. Saturn Blvd., Edwards AFB, CA 93524 (USA).

* To whom correspondence should be addressed. E-mail: pierangelo.metrangolo@polimi.it.

A well-known class of organic non-porous compounds, polymethylene bismethonium iodides, undergoes selective capture and release of α,ω-diiodoperfluoroalkanes in a dynamic and controlled manner, in solution and from the gas phase. Despite a lack of porosity of the starting materials, guest transport through the solid occurs readily until a thermodynamically stable porous structure is achieved, which is highly selective only to the convenient diiodoperfluoroalkane. The size matching between the inter-charge distance in the cation and the charge separation in the halogen-bonded $I^-\cdots I(CF_2)_mI\cdots I^-$ superanion drives the selectivity of the process, which identifies the target diiodoperfluoroalkane even from complex

industrial mixtures. The full reversibility of the process where diiodoperfluoroalkanes can first be selectively complexed and then quantitatively evacuated, yields pure fluorinated telomers and reusable decamethonium congeners.

α,ω-Diiodoperfluoroalkanes (DIPFAs) are key intermediates (*1*) for the synthesis of various fluorochemicals and fluoropolymers, *e.g.* fluorinated elastomers (*2-4*). However, the production of DIPFAs has been hampered by the lack of a method to obtain the compounds in high yield and purity. The tetrafluoroethylene telomerization reaction with iodine produces a mixture of DIPFAs, usually separated into its components by fractional distillation (*5*). The heavier DIPFAs cannot easily be separated by this method, therefore limiting the availability of α,ω-DIPFAs longer than eight carbon atoms.

In this paper, we report the application of supramolecular interactions and crystal engineering principles to the resolution of DIPFAs' mixtures through selective and reversible capturing by non-porous organic solids. In fact, the microcrystalline powder of polymethylene bismethonium iodides **1a-f**, by exposition to the vapors, rapidly and selectively incorporate only one of the α,ω-DIPFA **2a-f** (Scheme 1). Thus, **1a-f** represent a new class of virtually porous materials that selectively, dynamically, and in a controlled manner capture and release DIPFAs (*6*), through gas-solid processes or when the starting modules interact in solution.

We have already demonstrated that DIPFAs behave as robust telechelic halogen bonding (XB) (*7*,*8*) donors as fluorine boosts the electron density acceptor ability of iodine atoms

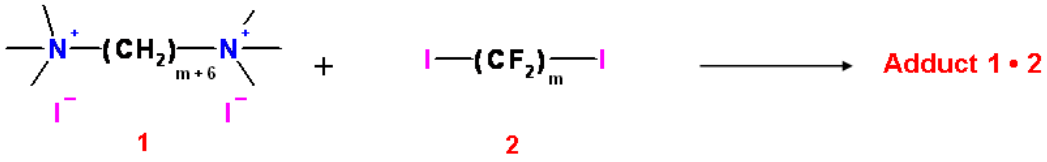

1, 2	a	b	c	d	e	f
m	2	4	6	8	10	12

Adduct	Distance A $^{+}N(CH_2)_{m+6}N^{+}$ (Å)	Distance B $I^{-}\cdots I(CF_2)_mI\cdots I^{-}$ (Å)	Δ (B - A) (Å)	
1a • 2a	11.343	12.142	0.799	MATCH
1b • 2b	13.617	14.483	0.866	
1c • 2c	16.395	17.083	0.688	
1b • 2d	13.746	18.796	5.050	MISMATCH
1a • 2b	10.535	14.105	3.570	

Scheme 1.

(*9*). For this reason, α,ω-DIPFAs give particularly strong halogen bonds when interacting with naked iodide ions (*10*), and result in trimeric supramolecular anions of the type $I^{-}\cdots I(CF_2)_mI\cdots I^{-}$, the length of which can be tuned by simply using DIPFAs of different length, *i.e.* varying m (*11*). As the binding is largely dependent on structural complementarity of the interacting charged moieties (*12*), we reasoned that matching the size of the halogen-bonded superanion with the use of a telechelic hydrocarbon (HC) dionium salt of similar dimensions should increase the strength of electrostatic binding, thus determining a selective molecular recognition of the target DIPFA. For this reason, we selected the iodide salts of the polymethylene bismethonium derivatives **1a-f** (*13*), which, besides their clinical use as potent neuromuscular blocking agents (*14*), are well-known

structure-directing agents in zeolite synthesis (*15*) and guests in supramolecular chemistry (*16*).

Single crystal X-ray analysis of the dihydrated of **1b** (Fig. 1, A) (*17*) shows that water is hydrogen-bonded to iodide ions ($H\cdots I^-$ distances 2.77-2.81 Å) and it interacts weakly also with the methyl and methylene H atoms of the cation. These interactions alongside the anion-cation interactions dominate the crystal structure. The decamethonium molecule adopts the usual *all-trans* conformation, and the HC chains are parallel and interdigitated.

The $N^+—N^+$ intramolecular distance in **1b** is 13.965 Å, which nicely fits to the $I^-—I^-$ distance in the $I^-\cdots I(CF_2)_4I\cdots I^-$ superanion, as found in our previous study (*18*). For this reason, we challenged **1b** with 1,4-diiodooctafluorobutane **2b**, starting from their equimolar CH_3OH and $CHCl_3$ solutions, respectively. Upon mixing the two solutions, the 1:1 supramolecular complex **1b·2b** was obtained in a nearly quantitative yield and purity. The single crystal X-ray analysis of the complex **1b·2b** confirms our initial hypothesis, and the distance between the intramolecular N atoms of **1b** in the complex matches with great accuracy the distance of the iodide ions in the superanion $I^-\cdots I(CF_2)_4I\cdots I^-$ (Δ = 0.866 Å, Scheme 1). Four HC cations define a rectangular parallelepiped, *i.e.* a molecular container, topped with two I^- ions, in the well-defined cavity of which the DIPFA **2b** is trapped due to the strong XB to the two I^- ions (Fig. 1, B and C). As a consequence of the optimized binding resulting from the structural complementarity of the interacting charged moieties and the matching sizes of the two starting compounds **1b** and **2b**, complex **1b·2b** shows a very high melting point and low solubility in organic solvents.

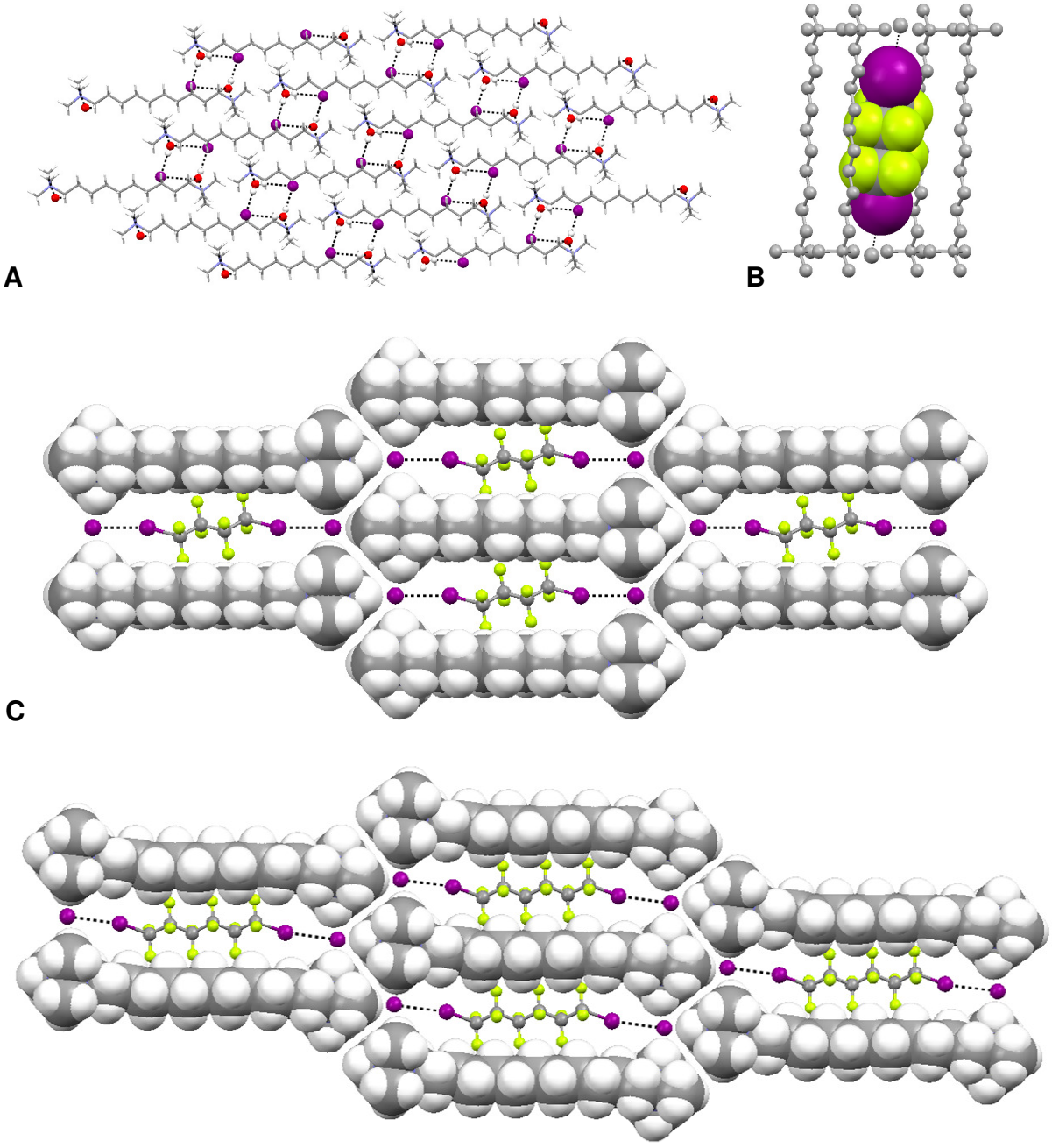

Fig. 1. (A) The packing of decamethonium iodide dihydrate **1b** viewed along the *a* axis; **(B)** The complex decamethonium iodide/diiodoperfluorobutane **1b**·**2b**: a view of the molecular container defined by four HC cations and topped by two I^- ions,

and the contained $I(CF_2)_4I$; **(C)** The crystal packing of the complex **1b·2b** viewed along the *c* axis; Only one of the disordered orientations of **2b** is shown; **(D)** The crystal packing of the complex **1c·2c** viewed along the *a* axis.

The $I^-\cdots$I-C distance of 3.452 Å and angle of 166.02° indicate strong XB (*7*), noticeably shorter than the sum of the van der Waals radius of iodine atom and the Pauling radius for the I^- ion (4.14 Å) (*19*).

To further test the size matching hypothesis, we challenged **1a** with **2a** and **1c** with **2c**, which should also be near in length, as they are the bisnor and bishomo analogues of **1b** and **2b**, respectively. Indeed, both of the complexes **1a·2a** (Fig. S1, Supporting Online Material) and **1c·2c** (Fig. 1, D) exhibit crystal lattices identical to that of the **1b·2b** complex. The 1,2-diiodotetrafluoroethane **2a** and the 1,6-diiodoperfluorohexane **2c** are trapped in a similar cavity surrounded by four HC chains and tightly bound by strong XB forming the superanions $I^-\cdots I(CF_2)_2I\cdots I^-$ ($I^-\cdots$I-C distance 3.478 Å, angle 167.18° in **1a·2a**) and $I^-\cdots I(CF_2)_6I\cdots I^-$ ($I^-\cdots$I-C distance 3.463 Å, angle 167.46° in **1c·2c**). Obeying the size matching between the interacting partners, the difference between the intramolecular N^+—N^+ distance and the charge separation in the $I^-\cdots I(CF_2)_mI\cdots I^-$ superanion is only 0.799 and 0.688 Å in **1a·2a** and **1c·2c**, respectively.

The importance of size matching of the interacting partners in the formation of these well-organized crystal lattices was confirmed by the crystal structures of two mismatching complexes, **1a·2b** and **1b·2d** (Scheme 1). In fact, the complex **1a·2b** revealed that, while

the formation of the discrete superanion $I^-\cdots I(CF_2)_4I\cdots I^-$ is preserved ($I^-\cdots$I-C distance 3.352 Å, angle 178.54°), the crystal packing is completely different from the **1a-c·2a-c** matching complexes. In **1a·2b**, due to the size mismatching between the cation and the superanion charge separations (3.57 Å), there is no cavity to trap the DIPFA inside and the structure consists of cation and superanion layers (Fig. S3, Supporting Online Material). Even greater is the difference for the complex **1b·2d**, whose stoichiometry is 1:2 and that shows, rather than a trimeric anion, an infinite 1D halogen-bonded polyanionic chain, with alternating **2d** molecules and I^- ions ($I^-\cdots$I-C distances 3.351 and 3.410 Å, angles 169.34 and 178.17°) (Fig. S4, Supporting Online Material). Here the mismatching between the dimensions of the dication and the superanion $I^-\cdots I(CF_2)_8I\cdots I^-$ was found to be as high as 5.050 Å.

All matching complexes, **1a·2a**, **1b·2b**, and **1c·2c**, show melting points higher than the mismatching ones in their respective homolog series. This is due to the high stability of these crystal lattices showing well-organized cavities around the DIPFAs. On the basis of the very low solubility and high melting points shown by the matching complexes compared to the mismatching ones, we surmised that the dimensional complementarity of the interacting charged moieties should determine a selective molecular recognition process in solution as a consequence of the increased strength of the electrostatic interactions (see onwards) (*11,20*).

With this in mind we performed competitive crystallization experiments by dissolving 1 eq of all the four commercially available α,ω-DIPFAs **2a-d** into the same $CHCl_3$ solution. As soon as this solution was added to a CH_3OH solution containing exclusively 1 eq of one

of the decamethonium congeners **1a-d**, only the size matching DIPFA was phased out from the solution and recovered with quantitative yield and purity. This was also the case for the 1,8-diiodoperfluorooctane **2d**, which was selectively phased out from a solution containing all the other DIPFAs by adding the tetradecamethonium iodide **1d**. Regardless of the fact that we were not able to obtain single crystal X-ray data for the complex **1d·2d**, the above described competitive crystallization experiment confirms that the size matching rule can be applied to any couple of compounds $\mathbf{1}_{m+6}$ and $\mathbf{2}_{m}$. Interestingly, once the matching DIPFA has been completely separated from the solution by filtration of the corresponding $\mathbf{1}_{m+6}\cdot\mathbf{2}_{m}$ solid adduct, the addition to the solution of another equivalent of the same decamethonium congener afforded always a white solid, which consisted of a mixture of all

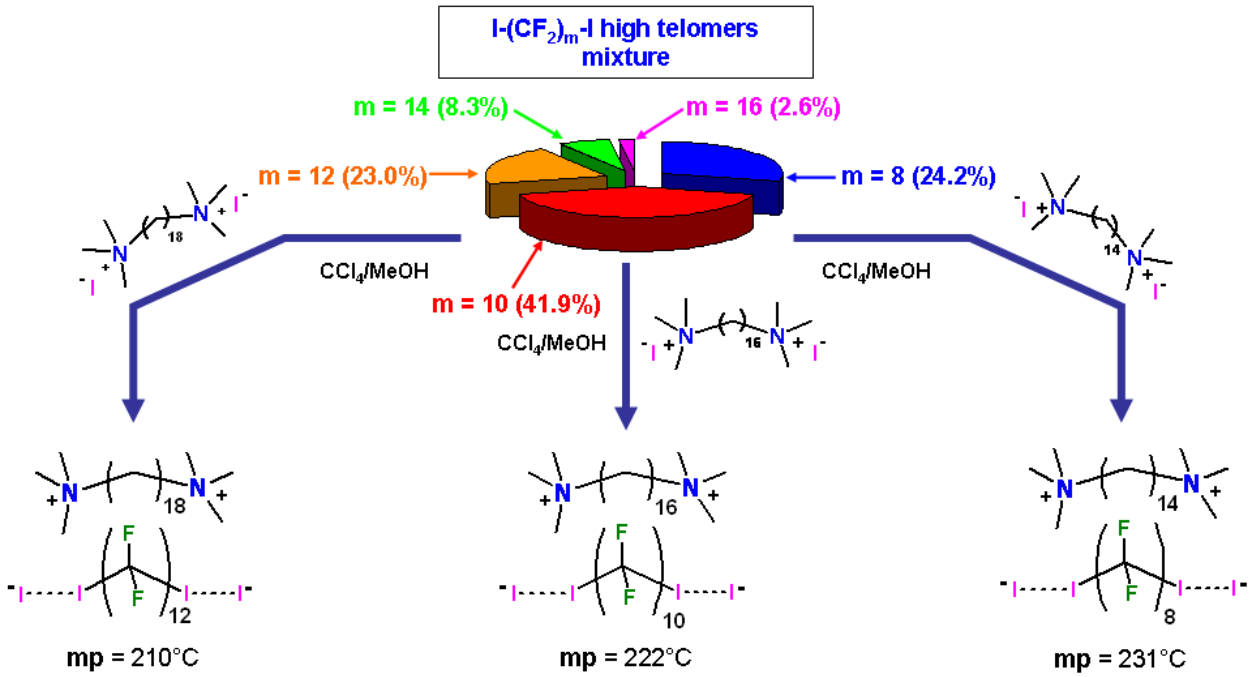

Scheme 2.

the other possible **1·2** mismatching complexes present in varying weight fractions.

Intrigued by the isolation of the **1d·2d** complex, we decided to apply the method of size matching with a suitable decamethonium congener to a mixture of higher DIPFA telomers (Scheme 2) found in a distillation residue from a typical industrial process having the following composition: 1,8-diiodoperfluorooctane **2d** (24.2%), 1,10-diiodoperfluorodecane **2e** (41.9%), 1,12-diiodoperfluorododecane **2f** (23.0%), 1,14-diiodoperfluorotetradecane (8.3%) and 1,16-diiodoperfluorohexadecane (2.6%). The α,ω-DIPFA mixture was dissolved in CCl_4 and a CH_3OH solution of hexadecamethonium iodide **1e** (1 eq for 1 eq of **2e** in the mixture) was added. A white solid precipitated almost immediately. Gas chromatography analysis indicated that **2e** was the only α,ω-DIPFA present in this solid (Fig. S16, Supporting Online Material). NMR experiments and melting point analysis on the solid confirmed the 1:1 ratio of the PFC and HC modules, and thus the formation of the complex **1e·2e**. The same experiment was repeated by adding to a solution of the DIPFA mixture, 1 eq of octadecamethonium iodide **1f**, obtaining the instantaneous precipitation of the almost pure (>90%) 1,12-diiodoperfluorododecane complex **1f·2f** (GC, NMR, IR, and melting point analysis), despite the low relative amount of **2f** in the starting mixture (23%). The poor solubility of the **1e·2e** and **1f·2f** complexes and their high melting points clearly confirmed the effectiveness of the size matching strategy, with the formation of complexes of the type $\mathbf{1_{m+6}{\cdot}2_m}$ also in the case of the very long telomers **2e** and **2f**. Thanks to the reversibility of XB and the high vapor pressure of DIPFAs, the target telomers can be sublimed off their bismethonium matching complexes in very high purity and yield.

To the best of our knowledge, no examples are available in the literature describing the detailed quantitative isolation of α,ω-DIPFAs as long as ten or twelve carbon atoms. Scattered examples report the isolation of analytical samples of **2e** and **2f** by gas chromatography (*21*). On the other hand, in the vast patent literature on the preparation of α,ω-DIPFAs, no evidence of separation methods other than time and energy consuming fractional distillation was found, with scarce indications of its effectiveness in the purification of the higher telomers (*22*).

The reversibility of the binding of the DIPFAs in our matching complexes was studied with various techniques. The gas phase IR experiments at ambient pressure in a sealed heating cell showed that the complex **1a·2a** starts to release **2a** at 160 °C (the boiling point of pure **2a** is 112 °C), with the maximum release occurring at 190 °C, well before the melting temperature of the complex (201 °C). This behavior was also proven for the other **1b-d·2b-d** matching complexes, which were studied similarly (DSC, DTA, and TG analyses); In addition, the powder X-ray diffraction (PXRD), IR, melting point, and NMR analyses confirmed that complete removal of **2a-c** yields the decamethonium congeners **1a-c** back in the same crystal phases of the starting materials. This confirms the full reversibility of the process where DIPFAs **2a-f** can first be selectively complexed and then quantitatively evacuated, thanks to their much higher vapor pressure than that of **1a-f**; This process yields pure isolated DIPFAs and reusable decamethonium congeners.

For practical and cleaner applications the selective size matching-based molecular recognition of DIFPAs should occur in non-solvent environment, thus we decided to study the reverse process, *viz.* the uptake of DIPFA vapors by the solid decamethonium

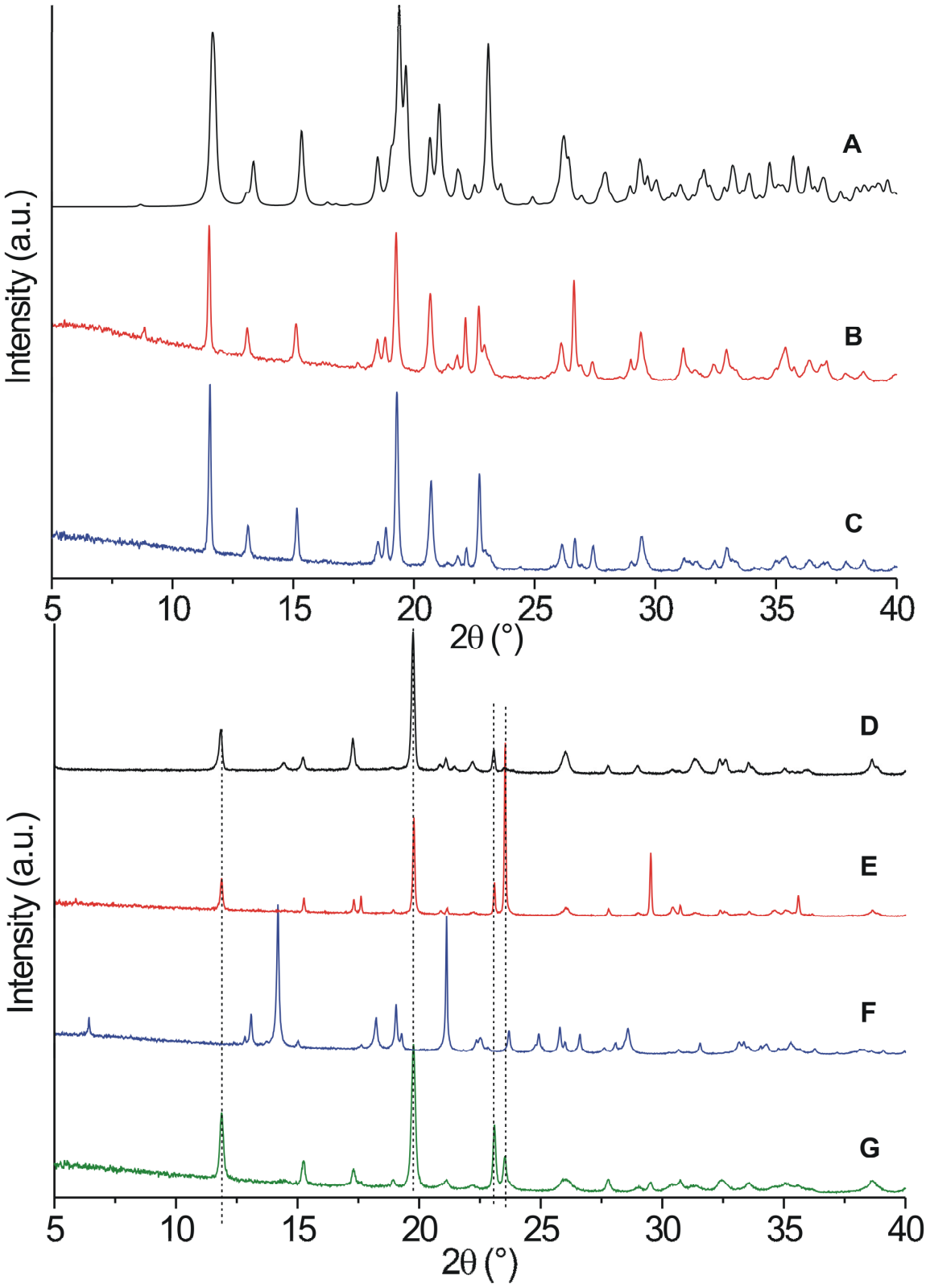
Intensity (a.u.)
A
B
C
5
10
15
20
25
30
35
40
2θ (°)
Intensity (a.u.)
D
E
F
G
5
10
15
20
25
30
35
40
2θ (°)

Fig. 2. Top; **(A)** PXRD patterns of the complex **1c·2c** simulated from single crystal X-ray data, **(B)** from solution crystallization, and **(C)** from gas-solid reaction. Bottom; PXRD patterns of the matching complex **1a·2a** obtained from solution crystallization, **(D)** before and **(E)** after exposure to vapors of 1,4-diiodoperfluorobutane **1b**. PXRD patterns of the mismatching complex **1a·2b** obtained from solution crystallization, **(F)** before and **(G)** after exposure to vapors of 1,2-diiodoperfluoroethane **1a**.

congeners. Finely ground decamethonium congeners **1a**, **1b**, or **1c** were placed in a sealed glass jar in the presence of liquid samples of the matching DIPFAs **2a**, **2b**, or **2c**, respectively, which were allowed to diffuse their vapors. The 1:1 matching complexes **1a·2a** and **1b·2b** were obtained after 6 hours and 7 days at ambient pressure and temperature, respectively, and both complexes had the same crystal lattices as those obtained from solution crystallization (Figs. S7 and S8, Supporting Online Material). Due to the lower vapor pressure of **1c**, the 1:1 matching complex **1c·2c** required 3 days at 40 °C to be obtained, and once again the same crystal phase as from solution was formed (Fig. 2, top). The gas-solid reactions described above transform the non-porous bismethonium iodides **1** into the corresponding $\mathbf{1}_{\mathbf{m+6}}\cdot\mathbf{2}_{\mathbf{m}}$ matching complexes thanks to lattice adaptation of the dication matrix, which organizes well-defined cavities around the superanion $I^-\cdots I(CF_2)_mI\cdots I^-$ only when the DIPFA $\mathbf{2}_{\mathbf{m}}$ has the opportune size, matching the linear dimensions of the dication $\mathbf{1}_{\mathbf{m+6}}$.

The selectivity of these gas-solid reactions has been further demonstrated by the following guest-exchange reaction. The finely ground mismatching complex **1a·2b**, as obtained from solution, was placed in a sealed glass jar in the presence of a liquid sample of the matching DIPFA **2a**, which was allowed to diffuse its vapors at ambient pressure and temperature for 7 days. The mismatching DIPFA **2b** was completely replaced in this gas-solid reaction by the matching one **2a**, yielding exclusively the 1:1 matching complex **1a·2a** in the same crystal form as obtained by solution crystallization (Fig. 2, F and G). The same experiment carried out on the matching complex **1a·2a** by exposure to vapors of the mismatching DIPFA **2b** did not result in any reaction (Fig. 2, D and E).

Nanoporous solids that are able to absorb and release small molecules in a controllable and selective fashion are rare but known in the literature (*23-27*). An alternative to nanoporosity is the controlled uptake and release of small molecules by means of reversible heterogeneous gas-solid reactions (*28-30*). We have shown that a well-known class of organic non-porous compounds, polymethylene bismethonium iodides **1a-f**, undergoes capture and release of the α,ω-DIPFAs **2a-f** in a dynamic, selective, and controlled manner, yielding the homologous series of supramolecular complexes $\mathbf{1}_{m+6}\cdot\mathbf{2}_m$, which obeys the precise size matching of the charged interacting partners. In solution, the size matching between the inter-charge distance in the cation and the charge separation in the halogen-bonded $I^-\cdots I(CF_2)_mI\cdots{}^-I$ superanion drives the selectivity of the process, which identifies the target DIPFA even from complex industrial mixtures. In gas-solid reactions, the formation of the matching complexes $\mathbf{1}_{m+6}\cdot\mathbf{2}_m$ is expected to involve surmounting a considerable energy barrier, especially in the case of the very long DIPFA **2c**, as it requires a dramatic

rearrangement of the whole structure of the crystalline decamethonium congeners. These reactions are likely to go through either a phase transition and rearrangement or in a well-orchestrated fashion (*23*). Despite a lack of porosity of the starting materials **1a-f**, the DIPFAs **2-f** are readily transported through the solid until a thermodynamically stable porous structure is achieved, which is highly selective only to the convenient DIPFA. A closer look at the X-ray structure of the pure decamethonium iodide **1b** (Fig. 1, A) suggests that once the DIPFA binds to the I^- ions via strong XB, the formation of the $I^-\cdots I(CF_2)_mI\cdots I^-$ superanion activates a size matching-induced allosteric process by facilitating a remarkable positional and/or orientational rearrangement of the HC cations (analogously to the sliding filament model similar to the one that occurs between thick and thin filaments in myofibrils). This unprecedented transformation of the host ionic lattice is triggered by the strong XB and the matching sizes of the charged interacting partners (*i.e.* the HC dication and the halogen-bonded superanion) (*12, 20*). The relevance of molecular imprinting in the selectivity of recognition processes is well established. Our results extend this relevance to the formation of porous materials through dynamic self-assembly.

Gas-solid reactions often imply profound transformations of the chemical and physical nature of the solid materials and rarely are of practical use. In our case, the full reversibility of the process, where DIPFA can first be selectively complexed and then quantitatively evacuated, yields pure fluorinated telomers and reusable decamethonium congeners. The reversibility of this process is important for the practical application of our discovery to the purification of a class of compounds of high commercial and industrial interest like the α,ω-DIPFAs (*31*). Ongoing studies in our laboratory are focusing on the application of this

purification method to another vast class of compounds of industrial interest, the α,ω-diiodoperfluoropolyethers (DIPFPEs), which are useful intermediates for the synthesis of fluoro-containing resins, elastomers, and surfactants (*32*).

References and Notes

1. N. O. Brace, *J. Fluorine Chem.* **108**, 147 (2001).
2. B. Ameduri, B. Boutevin, *Well-Architectured fluropolymers: Synthesis, Properties and Applications* Elsevier, Amsterdam, 2004.
3. K. Baum, T.G. Archibald, A.A. Malik, *J. Org. Chem.* **59**, 6804 (1994).
4. A. L. Logothetis in *Organofluorine Chemistry*, R. E. Banks, B. E. Smart, J. C. Tatlow Eds., Plenum Press, New York and London, 1994, pp. 373-396.
5. H.-P. Cao, Q.-Y. Chen, *J. Fluorine Chem.* **128**, 1187 (2007).
6. S. J. Dalgarno, P. K. Thallapally, L. J. Barbour, J. L. Atwood, *Chem. Soc. Rev.* **36**, 236 (2007).
7. P. Metrangolo, G. Resnati, *Chem. Eur. J.* **7**, 2511 (2001).
8. K. Rissanen, *CrystEngComm* **10**, 1107 (2008).
9. P. Metrangolo, G. Resnati, *Science* **321**, 9186 (2008).
10. P. Metrangolo, H. Neukirch, T. Pilati, G. Resnati, *Acc. Chem. Res.* **38**, 386 (2005).
11. P. Metrangolo, F. Meyer, T. Pilati, G. Resnati, G. Terraneo, *Angew. Chem. Int. Ed.* **47**, 6114 (2008).
12. M. I. Nelen, A. V. Eliseev, *J. Chem. Soc., Perkin Trans. 2* 1359 (1997).

13. H.-G. Löhr, A. Engel, H.-P. Josel, F. Vögtle, W. Schuh, H. Puff, *J. Org. Chem.* **49**, 1621 (1984).
14. C. Lee, T. Jones, *British J. Anaest.* **88**, 692 (2002).
15. P. Sun, Q. Jin, L. Wang, B. Li, D. Ding, *J. Porous Mater.* **10**, 145 (2003).
16. E. Menozzi, J. Rebek Jr., *Chem. Commun.* 5530 (2005).
17. Materials and methods are available as supporting material on *Science* Online.
18. R. Liantonio, P. Metrangolo, T. Pilati, G. Resnati, *Cryst. Growth Des.* **3**, 355 (2003).
19. A. Bondi, *J. Phys. Chem.* **68**, 441 (1964).
20. M. W. Hosseini, J. M. Lehn, *J. Am. Chem. Soc.* **104**, 3525 (1982).
21. S. Boneva, St. Kotov, *Chromatographia* **25**, 735 (1988).
22. H. Dindi, J. J. Hagedorn, M.-H. Hung, (to DuPont Dow Elastomers LLC (Wilmington, DE)) United States Patent 6825389 (30-11-2004).
23. J. L. Atwood, L. J. Barbour, A. Jerga, B. L. Schottel, *Science* **298**, 1000 (2002).
24. P. K. Thallapally, B. P. McGrail, S. J. Dalgarno, H. T. Schaef, J. Tian, J. L. Atwood, *Nature Mater.* **7**, 146 (2008).
25. B. D. Chandler, G. D. Enright, K. A. Udachin, S. Pawsey, J. A. Ripmeester, D. T. Cramb, G. K. H. Shimizu, *Nature Mater.* **7**, 229 (2008).
26. J. L. Atwood, L. J. Barbour, A. Jerga, *Science* **296**, 2367 (2002).
27. S. Kitagawa, K. Uemura, *Chem. Soc. Rev.* **34**, 109 (2005).

28. D. Braga, M. Curzi, A. Johansson, M. Polito, K. Rubini, F. Grepioni, *Angew. Chem. Int. Ed.* **45**, 142 (2006).
29. J. J. Vittal, *Coord. Chem. Rev.* **251**, 1781 (2007).
30. S. Libri, M. Mahler, G. Mìnguez Espallargas, D. C. N. G. Singh, J. Soleimannejad, H. Adams, M. D. Burgard, N. P. Rath, M. Brunelli, L. Brammer, *Angew. Chem. Int. Ed.* **47**, 1693 (2008).
31. Y. Carcenac, P. Metrangolo, G. Resnati, (to Politecnico di Milano) PCT/EP2008/058588 (03-07-2008), priority date (11-07-2007).
32. P.M., T.P., and G.R. gratefully wish to thank Fondazione Cariplo (Project "Self-Assembled Nanostructured Materials: A Strategy for the Control of Electrooptic Properties") for generous support. K.R. gratefully wish to thank the Academy of Finland (project no. 212588) for generous support. The authors declare no competing interests. Authors' contributions statement: experiments (A.V., Y.C., M.L., T.P., and P.M.), data analysis (P.M., G.R., K.R., M.L., T.P., and Y.C.), writing (P.M., G.R., K.R., M.L., and T.P.).

Supporting Online Material

www.sciencemag.org

Materials and Methods

Experimental Procedures

Further Results

Figs. S1 to S32

Tables S1 to S10

Schemes S1 to S2

References

Supporting Online Material

Materials and Methods

Commercial HPLC-grade solvents were used without further purification. Starting materials were purchased from Sigma–Aldrich, TCI Europe NV (**1b**), Acros Organics, and Apollo Scientific (**2a-d**). ^{1}H, and ^{13}C NMR spectra were recorded at ambient temperature on a Bruker AV-400 spectrometer, at 400 MHz and 100 MHz, respectively. ^{19}F NMR spectra were recorded at ambient temperature on a Bruker AV-500, at 470.6 MHz. All the chemical shifts are given in ppm. $CDCl_3$, CD_3OD, CD_3CN and DMSO-d_6 were used as both solvents and internal standards in ^{1}H NMR and ^{13}C NMR spectra. For ^{19}F NMR spectra, $CFCl_3$ was used as internal standard. Mass spectra were performed on a Bruker Esquire 3000 Plus spectrometer. IR spectra were obtained using a Nicolet Nexus FT-IR spectrometer equipped with UATR unit. Melting points were determined with a Reichert instrument by observing the melting and crystallizing process through an optical microscope. DSC analyses were carried out with a Linkam DSC600 hot stage (10 °C/min).

Single crystal data collection, structure solution and refinement

Data were collected on a Bruker SMART CCD diffractometer with Mo-Kα radiation. All the compounds, excluding pure **1b**, give very fragile crystals that possibly undergoes phase transition at low temperature. We always attempted to collect data at low temperature but it was possible to cool the crystals only for **1c·2c** (203 K) and **1a·2a** (253 K), using a OXFORD low temperature device. The structures were solved by *SIR*2002 (*S1*) and refined by *SHELXL*-97 (*S2*) programs, respectively. The refinement was carried on by full-matrix least-squares on F^2. Hydrogen atoms were placed using standard geometric models and with their thermal parameters riding on those of their parent atoms. All the complexes, excluding **1c·2c**, are disordered. In the complexes **1a·2a** and **1b·2b**, α,ω-DIPFAs are present in two opposite helical, nearly *all-trans* conformations, with great separation of fluorine atoms, so that the whole molecules could be split and refined with few restraints on the C-F geometry; as can be deduced comparing the ADPs of amino groups with those of the polymethilenic chains carbon atoms, also the latter are disordered, due to the strong interactions with the surrounding DIPFA molecules; notwithstanding, the separation of these carbon atoms is too low to allow their splitting and their restrained refinement. The situation of the mismatching complex **1a·2b** is similar, but the separation of carbon atoms in the octamethonium chain is greater, reaching 0.9 Å for the central atoms that were split. The situation of the complex **1b·2d** was definitely worst, being the crystals very poorly diffracting, so that the data collection was limited to 2θ = 37.4 °. Here the data/parameters ratio is very low but all the attempts to increase the data resolution by cooling the champions failed with crystal cracking, probably due to a 1st order phase transition. **1a·2a** crystals were very thin and 2θ was limited to 49.6 °.

Note: In contrast with all the other complexes and in pure **1b**, the conformation of the octamethonium chain of **1a** in the complex **1a·2b** is *tgtgt* rather than all-*trans.*

CCDC 709470 – 709475 contain the supplementary crystallographic data for this paper. These data can be obtained free of charge from The Cambridge Crystallographic Data Centre via www.ccdc.cam.ac.uk/data_request/cif.

Powder X-ray diffraction analysis

The powder X-ray diffraction data of the co-crystals and pure polymethylene bismethonium iodides were obtained at room temperature using PANalytical X´Pert PRO diffractometer. The measurements were made in Bragg–Brentano geometry using Johansson monochromator to produce pure CuKα_1 radiation (1.5406 Å; 45kV, 30mA) and step–scan technique in 2θ range of 3.5–72°. The data was acquired from a spinning sample by X´Celerator detector in continuous scanning mode with a step size of 0.0167° using sample dependently counting times of 40 to 440 s per step. Programmable divergence slit (PDS) was used in automatic mode to set irradiated length on sample to 15 mm together with 15 mm incident beam mask. Soller slits of 0.02° rad. were used on both incident and diffracted beam sides together with anti–scatter slits 4° and 13 mm, respectively. Lightly ground samples were prepared on a silicon-made zero–background holder using petrolatum jelly as an adhesive. The diffraction data were converted from automatic slit mode (ADS) to the fixed slit mode (FDS) data in PANalytical Highscore Plus v. 2.2c software package before further analyses. The simulated powder patterns used for comparison purposes were calculated by the program Mercury (*S3*) from the CIF-files of single crystal structures of expected complexes, when available. All the powder X-ray diffraction (PXRD) patterns that are presented in the paper are in most cases cut above 40°, though measured to 72° in 2θ, as the diffraction intensities decrease drastically on higher 2θ, thus not giving any significant information above given angle.

The Rietveld analyses were carried out for PXRD patterns of certain complexes using the Rietveld module implemented in PANalytical HighScore Plus program. In a typical Rietveld run, the structural parameters of analogous single crystal data taken from the CIF were used as a basis for the refinement. Refineable parameters were as follows: zero offset, scale factor, global displacement factor, profile parameters (U, V, W, η, asymmetry), cell parameters (axes and angles, when not strict by crystal system), atom parameters (x, y, z of heavier atoms only). Pseudo-Voigt function was used to describe the peak profiles and Chebyshev I function for baseline.

Thermal analysis

The thermal behavior of co-crystals (**1a-d·2a-d)** and pure polymethylene bismethonium iodides (**1a**-**1d**) were examined both with Perkin-Elmer PYRIS DIAMOND TG/DTA and/or TGA7 thermogravimetric analyzers. The measurements were carried out in platinum pans under synthetic air atmosphere (flow rates of 150 and 50 ml/min, respectively) with heating rates of 10 °C and 2 °C/min at a temperature range of 28–700 °C. In addition, isothermal runs were made by TGA7 at 190 °C (175 °C for **1d·2d**) for 60 min, to demonstrate complete removal of the DIPFA from a complexes clearly below its melting point. The temperature calibration was made using the melting points of five reference materials (In, Sn, Zn, Al, Au) on TG/DTA and Curie-point calibration technique (Alumel, Ni, Perkalloy, Fe) on TGA 7. On both instruments, the weight balance was calibrated by measuring the standard weight of 50 mg at room temperature. The sample weights used in the measurements were about 2–13 mg depending on the sample and the instrument used.

DSC measurements of certain samples (**1a-c·2a-c**) were carried out with Perkin Elmer Pyris Diamond DSC under flowing nitrogen (flow rate 50 ml/min) using 50 µl sealed aluminum

sample pan. The sealing was made by using a 30 µl aluminum pan with capillary holes as cover-pan to minimize a free volume inside a pan and to ascertain good thermal contact between a sample and pan. Extra pinhole was made to the center of a cover pan to ease the evaporation of the DIPFA in case of the measurements, in which slow heating rate was used. The temperature calibration was carried out using two standard materials (n-decane, In) and energy calibration by an indium standard (ΔH = 28.45 J/g). Various temperature profiles with heating rates of 3 and 10 °C/min were used to examine thermal behavior of the selected complexes. As an example for a temperature profile: a sample was consequently heated and cooled from 25 °C to a temperature few degrees above predetermined melting point at a rate of 10 °C/min and the cooled down to a room temperature with a cooling rate of 5 °C/min. Sample weights of about 2–5 mg were used in the measurements.

S1 A. Altomare, G. Cascarano, C. Giacovazzo, A. Guagliardi, M. C. Burla, G. Polidori, M. Camalli, *J. Appl. Crystallogr.*, **1994**, *27*, 435.
S2 G. M. Sheldrick, *SHELXL-97*, Program for refinement of crystal structures, University of Göttingen, Germany, **1997**.
S3 C. F. Macrae, P. R. Edgington, P. McCabe, E. Pidcock, G. P. Shields, R. Taylor, M. Towler and J. van de Streek, MERCURY, v1.5, *J. Appl. Crystallogr.*, **2006**, 39, 453.

Synthesis of starting hydrocarbon compounds

Tetradecane-1,14-diol (4e).
A solution of dodecanedicarboxylic acid **3e** (3.05 g, 11.8 mmol) in THF (50 mL) was added dropwise to a suspension of $LiAlH_4$ (1.85 g, 48.5 mmol) in THF (70 mL) at room temperature. The resulting mixture was stirred overnight, and iced water (5 mL) and aqueous sulphuric acid (10%, 50 mL) were successively carefully added. The organic phase was separated. The aqueous phase was extracted with ether two times. The combined organic phase was washed with sat. $NaHCO_3$ solution and then with brine, dried over sodium sulfate and concentrated under reduced pressure. The crude product was recrystallized in cyclohexane to give tetradecane-1,14-diol **4e** (2.69 g, 99%). White solid, m.p. 83°C. ^{1}H NMR (400 MHz, $CDCl_3$): δ 1.25-1.40 (m, 20H), 1.56 (m, 4H), 1.80 (s, 2H), 3.62 (t, 4H, *J*=6.6 Hz). ^{13}C NMR (100 MHz, $CDCl_3$): δ 21.9, 25.5, 28.1, 52.1, 65.2. I.R. (cm^{-1}): 3410, 3347, 2919, 2847, 1461, 1355, 1051, 1016, 972, 727.

Standard procedure for the synthesis of α,ω-diiodoalkanes 5:
Triphenylphosphine (6.82 g, 26 mmol) and imidazole (1.77 g, 26 mmol) were added to a solution of alkane-α,ω-diol **4** (10 mmol) in dichloromethane (60 mL) at 0°C. Iodine (6,60 g, 26 mmol) was slowly added and the reaction mixture was stirred at 0°C for 0.5 h, and then overnight at room temperature. Hexane (50 mL) was added and the resulting precipitate removed by filtration. The organic liquid was washed with water, dried on sodium sulfate and condensed. The residue was purified by silica gel chromatography (hexane).

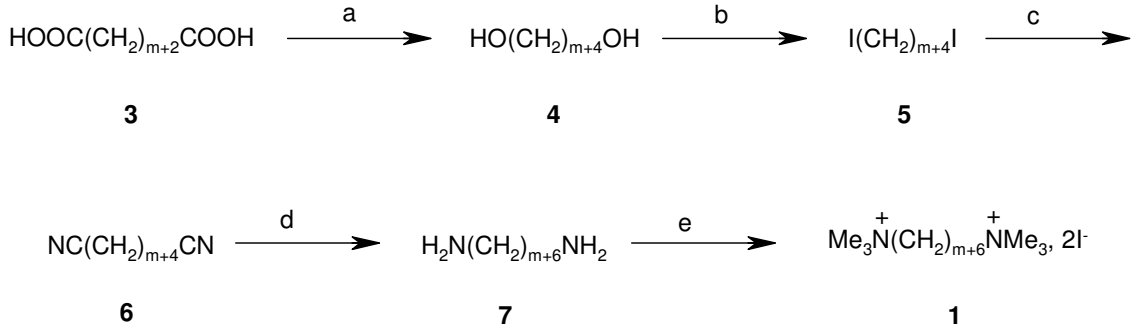

	a	b	c	d	e	f
m	2	4	6	8	10	12

Scheme S1. Synthesis of the polymethylene bismethonium iodides **1**. Reagents: (a) $LiAlH_4$; (b) PPh_3, I_2, imidazole; (c) n-$Bu_4N^+CN^-$; (d) $LiAlH_4$; (e) 1,2,2,6,6-pentamethylpiperidine, MeI; (f) PMe_3.

1,12-diiododododecane (5d).
95% yield, white solid, m.p. 38°C. ^{1}H NMR (400 MHz, $CDCl_3$): δ 1.26-1.34 (m, 12H), 1.40 (q, 4H, *J*=7.1 Hz), 1.83 (q, 4H, *J*=7.1 Hz), 3.19 (t, 4H, *J*=7.1 Hz). ^{13}C NMR (100 MHz, $CDCl_3$): δ 6.8, 28.5, 29.4, 29.5, 30.5, 33.6. I.R. (cm^{-1}): 2913, 2847, 1462, 1262, 1202, 1161, 718.

1,14-diiodotetradecane (5e).
81% yield, white solid, m.p. 44-46°C. ^{1}H NMR (400 MHz, $CDCl_3$): δ 1.25-1.32 (m, 16H), 1.39 (q, 4H, *J*=7.1 Hz), 1.82 (q, 4H, *J*=7.1 Hz), 3.19 (t, 4H, *J*=7.1 Hz). ^{13}C NMR (100 MHz, $CDCl_3$): δ 7.1, 28.5, 29.4, 29.5, 29.6, 30.5, 33.6. I.R. (cm^{-1}): 2913, 2846, 1462, 1248, 1196, 1162, 718.

Standard procedure for the synthesis of alkane-α,ω-dinitriles 6:
Tetrabutylammonium cyanide (4.03 g, 15 mmol) in dichloromethane (25 mL) was slowly added to a solution of α,ω-diiodoalkanes **5** (6 mmol) in dichloromethane (25 mL) at room temperature. The resulting mixture was stirred overnight. The solvent was removed and hexane (25 mL) was added. The resulting precipitate was removed by filtration and the organic liquid was washed with water, dried on sodium sulfate and concentrated under reduced pressure.

Dodecane-1,12-dinitrile (6d).
93% yield, white solid, m.p. 32-33°C. ^{1}H NMR (400 MHz, $CDCl_3$): δ 1.26-1.34 (m, 12H), 1.45 (q, 4H, *J*=7.2 Hz), 1.66 (q, 4H, *J*=7.2 Hz), 2.33 (t, 4H, *J*=7.2 Hz). ^{13}C NMR (100 MHz, $CDCl_3$): δ 17.1, 25.4, 28.6, 28.7, 29.2, 29.4, 119.7. I.R. (cm^{-1}): 2918, 2852, 2246, 1471, 718.

Tetradecane-1,14-dinitrile (6e).
90% yield, white solid, m.p. 45-46°C. ^{1}H NMR (400 MHz, $CDCl_3$): δ 1.25-1.35 (m, 16H), 1.44 (M, 4H), 1.65 (q, 4H, *J*=7.2 Hz), 2.32 (t, 4H, *J*=7.2 Hz). ^{13}C NMR (100 MHz, $CDCl_3$): δ 17.1, 25.3, 28.6, 28.7, 29.2, 29.4, 29.5, 119.7. I.R. (cm^{-1}): 2916, 2850, 2247, 1473, 717.

Standard procedure for the synthesis of alkane-α,ω-diamines 7:
A solution of alkane-α,ω-dinitrile **6** (3.25 mmol) in ether (20 mmol) was added dropwise to a suspension of $LiAlH_4$ (500 mg, 13.2 mmol) in ether (20 mL) at room temperature. The resulting mixture was refluxed for 0.5 h, cooled to room temperature and stirred overnight. Iced water (5 mL) was carefully added. The resulting precipitate was removed by filtration and washed with ether. The organic liquid was separated, washed with brine, dried on sodium sulfate and concentrated under reduced pressure.

Tetradecane-1,14-diamine (7d).
88% yield, white solid, m.p. 66°C. ^{1}H NMR (400 MHz, CD_3OD): δ 1.37-1.44 (m, 24H), 1.56 (m, 4H), 2.72 (t, 4H, *J*=7.1 Hz). ^{13}C NMR (100 MHz, CD_3OD): δ 28.1, 30.6, 30.7, 30.7, 30.8, 33.9, 42.6. I.R. (cm^{-1}): 3330, 3164, 2917, 2848, 1606, 1462, 1006, 925, 896, 720.

Hexadecane-1,16-diamine (7e).

65% yield, white solid, m.p. 74°C. ^{1}H NMR (400 MHz, $CDCl_3$): δ 1.20-1.36 (m, 28H), 1.43 (m, 4H), 2.67 (t, 4H, *J*=7.0 Hz). ^{13}C NMR (100 MHz, $CDCl_3$): δ 26.8, 29.1, 29.6 (4C), 33.9, 42.3. I.R. (cm^{-1}): 3348, 2914, 2848, 1571, 1471, 981, 951, 716.

Standard procedure for the synthesis of the polymethylene bismethonium iodides 1:
3.8 mL (61 mmol) of methyl iodide were added dropwise at ambient temperature to a mixture of diamine **7** (5 mmol) and 1,2,2,6,6-pentamethylpiperidine (20 mmol) in DMF (25 mL). The reaction mixture was stirred overnight at room temperature to ensure complete precipitation of the bisquaternary compound. The resulting solid was then filtered, washed with acetone and dried under vacuum to give the pure product.

Octamethonium iodide (1a).
84% yield, white solid, m.p. 265°C. ^{1}H NMR (400 MHz, DMSO): δ 1.23-1.38 (m, 8H), 1.68 (m, 4H), 3.06 (s, 18H), 3.28 (m, 4H). ^{13}C NMR (100 MHz, DMSO): δ 21.9, 25.5, 28.1, 52.1, 65.2. ESI-MS, positive-ion mode: m/z 357 [M - I], 115 [M - 2I]. I.R. (cm^{-1}): 3012, 2929, 2857, 1475, 1465, 966, 955, 921, 907.

Decamethonium iodide (1b).
White solid, m.p. 250°C. I.R. (cm^{-1}): 3484, 3432, 3004, 2923, 2858, 1628, 1492, 1479, 964, 910, 731, 714.

Dodecamethonium iodide (1c).
82% yield, white solid, m.p. 222°C. ^{1}H NMR (400 MHz, DMSO): δ 1.22-1.35 (m, 16H), 1.66 (m, 4H), 3.05 (s, 18H), 3.28 (m, 4H). ^{13}C NMR (100 MHz, DMSO): δ 21.9, 25.5, 28.3, 28.6, 28.7, 52.0, 65.2. ESI-MS, positive-ion mode: m/z 413 [M - I], 143 [M - 2I]. I.R. (cm^{-1}): 3002, 2914, 2851, 1483, 1464, 973, 939, 916, 731.

Tetradecamethonium iodide (1d).
59% yield, white solid, m.p. 207°C. ^{1}H NMR (400 MHz, CD_3CN): δ 1.28-1.36 (m, 20H), 1.72 (m, 4H), 3.06 (s, 18H), 3.28 (m, 4H). ^{13}C NMR (100 MHz, CD_3CN): δ 23.4, 26.7, 29.6, 30.0, 30.1, 30.2, 53.9, 67.6. ESI-MS, positive-ion mode: m/z 441 [M - I], 157 [M - 2I]. I.R. (cm^{-1}): 3004, 2917, 2852, 1482, 1464, 972, 951, 921, 897, 733.

Hexadecamethonium iodide (1e).
62% yield, white solid, m.p. 114°C. ^{1}H NMR (400 MHz, CD_3OD): δ 1.30-1.45 (m, 24H), 1.79 (m, 4H), 3.14 (s, 18H), 3.35 (m, 4H). ^{13}C NMR (100 MHz, CD_3OD): δ 24.0, 27.4, 30.2, 30.5, 30.6, 30.7, 30.8, 53.8, 68.1. ESI-MS, positive-ion mode: m/z 469 [M - I], 171 [M - 2I]. I.R. (cm^{-1}): 3003, 2919, 2849, 1485, 1465, 952, 911, 719.

Synthesis of the octadecamethonium iodide (1f).

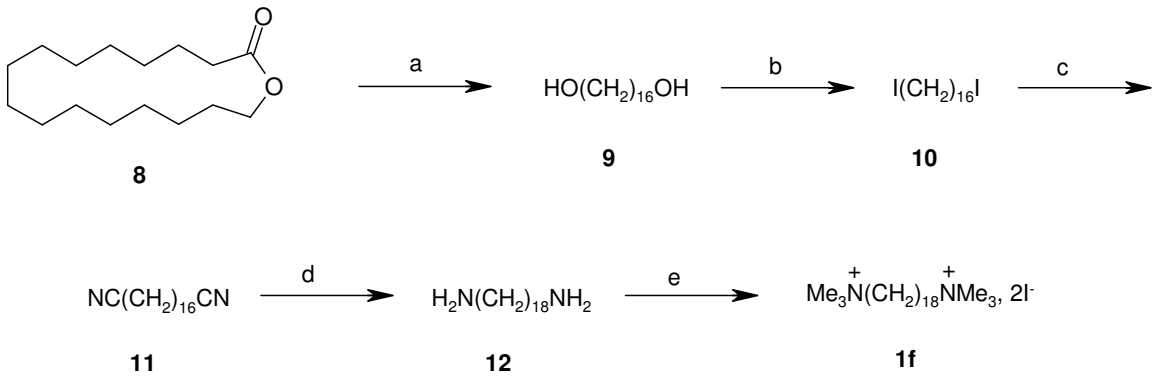

Scheme 1. Synthesis of the octadecamethonium iodide **1f**. Reagents: (a) $LiAlH_4$; (b) PPh_3, I_2, imidazole; (c) $n$$Bu_4N^+CN^-$; (d) $LiAlH_4$; (e) 1,2,2,6,6-pentamethylpiperidine, MeI.

Hexadecane-1,16-diol (9).
A solution of hexadecanolide **8** (5.18 g, 20.4 mmol) in THF (25 mL) was added dropwise to a suspension of $LiAlH_4$ (2.33 g, 61.3 mmol) in THF (50 mL) at room temperature. The resulting mixture was refluxed during 2h, hydrolyzed with NaOH 15% (15 mL), and refluxed again during 1h and filtered. The residue was extracted with THF. The combined organic phases were washed with brine, dried over sodium sulfate and concentrated under reduced pressure. 5.23 g of hexadecane-1,16-diol were obtained (99%). White solid, m.p. 89-90°C. ^{1}H NMR (400 MHz, $CDCl_3$): δ 1.24-1.38 (m, 24H), 1.57 (m, 4H), 3.64 (t, 4H, J=6.7 Hz). ^{13}C NMR (100 MHz, $CDCl_3$): δ25.7, 29.4, 29.5, 29.6 (3), 32.8, 63.1.

1,16-diiodohexadecane (10).
Triphenylphosphine (13.53 g, 51.6 mmol) and imidazole (3.51 g, 51.6 mmol) were added to a solution of **9** (19.85 mmol) in dichloromethane (120 mL) at 0°C. Iodine (13.10 g, 51.6 mmol) was slowly added and the reaction mixture was stirred at 0°C for 0.5 h, and then overnight at room temperature. Hexane (100 mL) was added and the resulting precipitate removed by filtration. The organic liquid was washed with water, dried on sodium sulfate and condensed. The residue was purified by silica gel chromatography (hexane) to give 5.55 g of 1,16-diiodohexadecane (59%). White solid, m.p. 48-50°C. ^{1}H NMR (400 MHz, $CDCl_3$): δ 1.24-1.33 (m, 20H), 1.39 (m, 4H), 1.83 (m, 4H), 3.19 (t, 4H, J=7.1 Hz). ^{13}C NMR (100 MHz, $CDCl_3$): δ7.1, 28.5, 29.4, 29.5, 29.6 (2), 30.5, 33.6.

Hexadecane-1,16-dinitrile (11).
Tetrabutylammonium cyanide (6.55 g, 24.4 mmol) in dichloromethane (50 mL) was slowly added to a solution of **10** (10.92 mmol) in dichloromethane (50 mL) at room temperature. The resulting mixture was stirred overnight. The solvent was removed and hexane (25 mL) was added. The resulting precipitate was removed by filtration and the organic liquid was washed with water, dried on sodium sulfate and concentrated under reduced pressure. 2.78 g of Hexadecane-1,16-dinitrile were obtained (92%). White solid, m.p. 54-56°C. ^{1}H NMR

(400 MHz, $CDCl_3$): δ 1.25-1.35 (m, 20H), 1.45 (m, 4H), 1.65 (m, 4H), 2.32 (t, 4H, J=7.1 Hz). ^{13}C NMR (100 MHz, $CDCl_3$): δ 17.1, 25.4, 28.6, 28.7, 29.3, 29.5 (2), 29.6, 119.7.

Octadecane-1,18-diamine (12).
A solution of **11** (9.4 mmol) in ether (60 mmol) was added dropwise to a suspension of $LiAlH_4$ (1.43 g, 37.6 mmol) in ether (60 mL) at room temperature. The resulting mixture was refluxed during 2h, hydrolyzed with 2M NaOH and refluxed again for 1h. The resulting precipitate was removed by filtration on celite and washed with ether. The organic liquid was separated, washed with brine, dried on sodium sulfate and concentrated under reduced pressure. 675 mg of octadecane-1,18-diamine is obtained (white solid, 60%).

Octadecamethonium iodide (1f).
3.65 g (25.7 mmol) of methyl iodide were added dropwise at ambient temperature to a mixture of **12** (600 mg, 2.11 mmol) and 1,2,2,6,6-pentamethylpiperidine (1.33 g, 8.56 mmol) in acetone (20 mL). The reaction mixture was stirred overnight at room temperature to ensure complete precipitation of the bisquaternary compound. The resulting solid was then filtered, washed with acetone and dried under vacuum. ^1H NMR (400 MHz, CD_3OD): δ 1.25-1.40 (m, 28H), 1.79 (m, 4H), 3.13 (s, 18H), 3.35 (m, 4H). ^{13}C NMR (100 MHz, CD_3OD): δ 24.0, 27.4, 30.2, 30.5 (2), 30.6, 30.7, 30.8, 53.7, 68.1.

General procedure for the synthesis of the complexes 1·2:
Equimolar amounts of diiodoperfluoroalkane and polymethylene bismethonium iodide were solubilized separately, in chloroform or carbon tetrachloride and in acetonitrile or methanol, respectively. The two solutions were mixed in a vial which was closed in a closed glass jar containing paraffine oil. Volatile solvents were allowed to diffuse at room temperature until crystals were formed, which were filtered and washed with fresh solvent.

Complex 1a·2a formed by octamethonium iodide and 1,2-diiodotetrafluoroethane.
White solid, m.p. 201°C. I.R. (cm^{-1}, selected bands): pure octamethonium iodide: 3012, 2929, 2857, 1475, 1465, 966, 955, 921, 907; pure 1,2-diiodotetrafluoroethane: 1147, 1096, 973, 834, 689; co-crystal: 3011, 2945, 2872, 2854, 1477, 1405, 1128, 1090, 950, 905, 693. ^{19}F NMR (470.6 MHz, CD_3OD, 0.002 M): pure 1,2-diiodotetrafluoroethane: δ_F -56.24; co-crystal : $\Delta\delta_F = 0.02$.

Complex 1a·2b formed by octamethonium iodide and 1,4-diiodoperfluorobutane.
White solid, m.p. 188°C. I.R. (cm^{-1}, selected bands): pure octamethonium iodide: 3012, 2929, 2857, 1475, 1465, 966, 955, 921, 907; pure 1,4-diiodoperfluorobutane: 1190, 1130, 1039, 887, 763; co-crystal: 3015, 2929, 2862, 1488, 1450, 1178, 1128, 1042, 954, 910, 759. ^{19}F NMR (470.6 MHz, CD_3OD, 0.002 M): pure 1,4-diiodoperfluorobutane: δ -63.80 ($IC\mathit{F}_2CF_2)_2$, -112.02 ($ICF_2C\mathit{F}_2)_2$; co-crystal: $\Delta\delta_{(IC\mathit{F}2CF2)2} = 0.03$, $\Delta\delta_{(ICF2C\mathit{F}2)2} = 0.00$.

Complex 1a·2c formed by octamethonium iodide and 1,6-diiodoperfluorohexane.
White solid, m.p. 182°C. I.R. (cm^{-1}, selected bands): pure octamethonium iodide: 3012, 2929, 2857, 1475, 1465, 966, 955, 921, 907; pure 1,6-diiodoperfluorohexane: 1200, 1142, 1087, 924, 783, 763; co-crystal: 3014, 2929, 2861, 1478, 1198, 1148, 1082, 955, 911, 778, 760. ^{19}F NMR (470.6 MHz, CD_3OD, 0.002 M): pure 1,6-diiodoperfluorohexane: δ -64.49 ($IC\mathit{F}_2CF_2CF_2)_2$, -113.02 ($ICF_2C\mathit{F}_2CF_2)_2$, -120.26 ($ICF_2CF_2C\mathit{F}_2)_2$; co-crystal : $\Delta\delta_{(IC\mathit{F}2CF2CF2)2} = 0.09$, $\Delta\delta_{(ICF2C\mathit{F}2CF2)2} = 0.01$, $\Delta\delta_{(ICF2CF2C\mathit{F}2)2} = 0.00$.

Complex 1a·2d formed by octamethonium iodide and 1,8-diiodoperfluorooctane.
White solid, m.p. 178°C. I.R. (cm^{-1}, selected bands): pure octamethonium iodide: 3012, 2929, 2857, 1475, 1465, 966, 955, 921, 907; pure 1,8-diiodoperfluorooctane: 1203, 1145, 1112, 1090, 1055, 833; co-crystal: 3010, 2928, 2854, 1489, 1477, 1208, 1147, 1132, 1108, 1089, 1055, 957, 910, 827. ^{19}F NMR (470.6 MHz, CD_3OD, 0.002 M): pure 1,8-diiodoperfluorooctane: δ -64.71 ($IC\mathit{F}_2CF_2CF_2CF_2)_2$, -113.01 ($ICF_2C\mathit{F}_2CF_2CF_2)_2$, -120.20 ($ICF_2CF_2C\mathit{F}_2CF_2)_2$, -121.05 ($ICF_2CF_2CF_2C\mathit{F}_2)_2$; co-crystal: $\Delta\delta_{(IC\mathit{F}2CF2CF2CF2)2} = 0.06$, $\Delta\delta_{(ICF2C\mathit{F}2CF2CF2)2} = 0.02$, $\Delta\delta_{(ICF2CF2C\mathit{F}2CF2)2} = 0.01$, $\Delta\delta_{(ICF2CF2CF2C\mathit{F}2)2} = 0.00$.

Complex 1b·2a formed by decamethonium iodide and 1,2-diiodotetrafluoroethane.
White solid, m.p. 140°C. I.R. (cm^{-1}, selected bands): pure decamethonium iodide: 3002, 2923, 2859, 1628, 1492, 1479, 964, 950, 910, 714; pure 1,2-diiodotetrafluoroethane: 1147, 1096, 973, 834, 689; co-crystal: 3010, 2924, 2858, 1629, 1477, 1417, 1121, 1086, 963, 908, 688. ^{19}F NMR (470.6 MHz, CD_3OD, 0.002 M): pure 1,2-diiodotetrafluoroethane: δ -56.24; co-crystal : $\Delta\delta_F = 0.06$.

Complex 1b·2b formed by decamethonium iodide and 1,4-diiodoperfluorobutane.
White solid, m.p. 230°C. I.R. (cm^{-1}, selected bands): pure decamethonium iodide: 3002, 2923, 2859, 1628, 1492, 1479, 964, 950, 910, 714; pure 1,4-diiodoperfluorobutane: 1190, 1130, 1039, 887, 763; co-crystal: 3010, 2941, 2870, 1475, 1405, 1184, 1123, 1040, 961, 761. ^{19}F NMR (470.6 MHz, CD_3OD, 0.002 M): pure 1,4-diiodoperfluorobutane: δ -63.80 ($IC\mathit{F}_2CF_2)_2$, -112.02 ($ICF_2C\mathit{F}_2)_2$; co-crystal: $\Delta\delta_{(IC\mathit{F}2CF2)2} = 0.02$, $\Delta\delta_{(ICF2C\mathit{F}2)2} = 0.00$.

Complex 1b·2c formed by decamethonium iodide and 1,6-diiodoperfluorohexane.
White solid, m.p. 191°C. I.R. (cm^{-1}, selected bands): pure decamethonium iodide: 3002, 2923, 2859, 1628, 1492, 1479, 964, 950, 910, 714; pure 1,6-diiodoperfluorohexane: 1200, 1142, 1087, 924, 783, 763; co-crystal: 3008, 2945, 2868, 1476, 1409, 1197, 1136, 1079, 954, 899, 781, 763. ^{19}F NMR (470.6 MHz, CD_3OD, 0.002 M): pure 1,6-diiodoperfluorohexane: δ -64.49 ($IC\mathit{F}_2CF_2CF_2)_2$, -113.02 ($ICF_2C\mathit{F}_2CF_2)_2$, -120.26 ($ICF_2CF_2C\mathit{F}_2)_2$; co-crystal: $\Delta\delta_{(IC\mathit{F}2CF2CF2)2} = 0.08$, $\Delta\delta_{(ICF2C\mathit{F}2CF2)2} = -0.03$, $\Delta\delta_{(ICF2CF2C\mathit{F}2)2} = -0.02$.

Complex 1b·2d formed by decamethonium iodide and 1,8-diiodoperfluorooctane.
White solid, m.p. 132°C. I.R. (cm^{-1}, selected bands): pure decamethonium iodide: 3002, 2923, 2859, 1628, 1492, 1479, 964, 950, 910, 714; pure 1,8-diiodoperfluorooctane: 1203, 1145, 1112, 1090, 1055, 833; co-crystal: 3004, 2934, 2860, 1485, 1473, 1213, 1186, 1147, 1119, 1102, 1081, 963, 905, 829. ^{19}F NMR (470.6 MHz, CD_3OD, 0.002 M): pure 1,8-diiodoperfluorooctane: δ -64.71 ($IC\mathit{F}_2CF_2CF_2CF_2)_2$, -113.01 ($ICF_2C\mathit{F}_2CF_2CF_2)_2$, -120.20 ($ICF_2CF_2C\mathit{F}_2CF_2)_2$, -121.05 ($ICF_2CF_2CF_2C\mathit{F}_2)_2$; co-crystal: $\Delta\delta_{(IC\mathit{F}2CF2CF2CF2)2} = 0.11$, $\Delta\delta_{(ICF2C\mathit{F}2CF2CF2)2} = 0.01$, $\Delta\delta_{(ICF2CF2C\mathit{F}2CF2)2} = 0.01$, $\Delta\delta_{(ICF2CF2CF2C\mathit{F}2)2} = 0.00$.

Complex 1c·2a formed by dodecamethonium iodide and 1,2-diiodotetrafluoroethane.
White solid, m.p. 128°C. I.R. (cm^{-1}, selected bands): pure dodecamethonium iodide: 3002, 2914, 2851, 1483, 1464, 973, 939, 916, 731; pure 1,2-diiodotetrafluoroethane: 1147, 1096, 973, 834, 689; co-crystal: 3007, 2925, 2852, 1477, 1406, 1122, 1090, 966, 934, 907, 726, 691. ^{19}F NMR (470.6 MHz, CD_3OD, 0.002 M): pure 1,2-diiodotetrafluoroethane: δ -56.24; co-crystal: $\Delta\delta_F = 0.03$.

Complex 1c·2b formed by dodecamethonium iodide and 1,4-diiodoperfluorobutane.
White solid, m.p. 217°C. I.R. (cm^{-1}, selected bands): pure dodecamethonium iodide: 3002, 2914, 2851, 1483, 1464, 973, 939, 916, 731; pure 1,4-diiodoperfluorobutane: 1190, 1130, 1039, 887, 763; co-crystal: 3011, 2927, 2855, 1481, 1406, 1193, 1121, 1040, 964, 907, 761, 729. ^{19}F NMR (470.6 MHz, CD_3OD, 0.002 M): pure 1,4-diiodoperfluorobutane: δ -63.80 ($IC\mathit{F}_2CF_2)_2$, -112.02 ($ICF_2C\mathit{F}_2)_2$; co-crystal: $\Delta\delta_{(IC\mathit{F}2CF2)2} = 0.03$, $\Delta\delta_{(ICF2C\mathit{F}2)2} = 0.00$.

Complex 1c·2c formed by dodecamethonium iodide and 1,6-diiodoperfluorohexane.
White solid, m.p. 227°C. I.R. (cm^{-1}, selected bands): pure dodecamethonium iodide: 3002, 2914, 2851, 1483, 1464, 973, 939, 916, 731; pure 1,6-diiodoperfluorohexane: 1200, 1142, 1087, 924, 783, 763; co-crystal: 3010, 2941, 2867, 1475, 1405, 1203, 1141, 1125, 1081,

963, 928, 909, 731. ^{19}F NMR (470.6 MHz, CD_3OD, 0.002 M): pure 1,6-diiodoperfluorohexane: δ -64.49 ($IC\mathit{F}_2CF_2CF_2)_2$, -113.02 ($ICF_2C\mathit{F}_2CF_2)_2$, -120.26 ($ICF_2CF_2C\mathit{F}_2)_2$; co-crystal: $\Delta\delta_{(IC\mathit{F}2CF2CF2)2}$ = 0.08, $\Delta\delta_{(ICF2C\mathit{F}2CF2)2}$ = 0.01, $\Delta\delta_{(ICF2CF2C\mathit{F}2)2}$ = 0.00.

Complex 1c·2d formed by dodecamethonium iodide and 1,8-diiodoperfluorooctane.
White solid, m.p. 191°C. I.R. (cm^{-1}, selected bands): pure dodecamethonium iodide: 3002, 2914, 2851, 1483, 1464, 973, 939, 916, 731; pure 1,8-diiodoperfluorooctane: 1203, 1145, 1112, 1090, 1055, 833; co-crystal: 3008, 2935, 2864, 1475, 1204, 1145, 1105, 1080, 1055, 964, 930, 902, 833, 738. ^{19}F NMR (470.6 MHz, CD_3OD, 0.002 M): pure 1,8-diiodoperfluorooctane: δ -64.71 ($IC\mathit{F}_2CF_2CF_2CF_2)_2$, -113.01 ($ICF_2C\mathit{F}_2CF_2CF_2)_2$, -120.20 ($ICF_2CF_2C\mathit{F}_2CF_2)_2$, -121.05 ($ICF_2CF_2CF_2C\mathit{F}_2)_2$; co-crystal: $\Delta\delta_{(IC\mathit{F}2CF2CF2CF2)2}$ = 0.05, $\Delta\delta_{(ICF2C\mathit{F}2CF2CF2)2}$ = 0.01, $\Delta\delta_{(ICF2CF2C\mathit{F}2CF2)2}$ = 0.01, $\Delta\delta_{(ICF2CF2CF2C\mathit{F}2)2}$ = 0.00.

Complex 1d·2a formed by tetradecamethonium iodide and 1,2-diiodotetrafluoroethane.
White solid, m.p. 124°C. I.R. (cm^{-1}, selected bands): pure tetradecamethonium iodide: 3004, 2917, 2852, 1482, 1464, 972, 951, 921, 897, 733; pure 1,2-diiodotetrafluoroethane: 1147, 1096, 973, 834, 689; co-crystal: 3004, 2923, 2853, 1481, 1136, 1094, 966, 904, 724, 694. ^{19}F NMR (470.6 MHz, CD_3OD, 0.002 M): pure 1,2-diiodotetrafluoroethane: δ -56.24; co-crystal: $\Delta\delta_F$ = 0.11.

Complex 1d·2b formed by tetradecamethonium iodide and 1,4-diiodoperfluorobutane.
White solid, m.p. 181°C. I.R. (cm^{-1}, selected bands): pure tetradecamethonium iodide: 3004, 2917, 2852, 1482, 1464, 972, 951, 921, 897, 733; pure 1,4-diiodoperfluorobutane: 1190, 1130, 1039, 887, 763; co-crystal: 3010, 2924, 2855, 1484, 1181, 1126, 1040, 966, 909, 761, 722. ^{19}F NMR (470.6 MHz, CD_3OD, 0.002 M): pure 1,4-diiodoperfluorobutane: δ -63.80 ($IC\mathit{F}_2CF_2)_2$, -112.02 ($ICF_2C\mathit{F}_2)_2$; co-crystal: $\Delta\delta_{(IC\mathit{F}2CF2)2}$ = 0.13, $\Delta\delta_{(ICF2C\mathit{F}2)2}$ = 0.01.

Complex 1d·2c formed by tetradecamethonium iodide and 1,6-diiodoperfluorohexane.
White solid, m.p. 231°C. I.R. (cm^{-1}, selected bands): pure tetradecamethonium iodide: 3004, 2917, 2852, 1482, 1464, 972, 951, 921, 897, 733; pure 1,6-diiodoperfluorohexane: 1200, 1142, 1087, 924, 783, 763; co-crystal: 3010, 2929, 2857, 1473, 1214, 1137, 1081, 963, 946, 924, 908, 779, 727, 692. ^{19}F NMR (470.6 MHz, CD_3OD, 0.002 M): pure 1,6-diiodoperfluorohexane: δ -64.49 ($IC\mathit{F}_2CF_2CF_2)_2$, -113.02 ($ICF_2C\mathit{F}_2CF_2)_2$, -120.26 ($ICF_2CF_2C\mathit{F}_2)_2$; co-crystal: $\Delta\delta_{(IC\mathit{F}2CF2CF2)2}$ = 0.06, $\Delta\delta_{(ICF2C\mathit{F}2CF2)2}$ = 0.01, $\Delta\delta_{(ICF2CF2C\mathit{F}2)2}$ = 0.00.

Complex 1d·2d formed by tetradecamethonium iodide and 1,8-diiodoperfluorooctane.
White solid, m.p. 231°C. I.R. (cm^{-1}, selected bands): pure tetradecamethonium iodide: 3004, 2917, 2852, 1482, 1464, 972, 951, 921, 897, 733; pure 1,8-diiodoperfluorooctane: 1203, 1145, 1112, 1090, 1055, 833; co-crystal: 3010, 2940, 2865, 1475, 1210, 1146, 1105, 1056, 959, 905, 827, 731. ^{19}F NMR (470.6 MHz, CD_3OD, 0.002 M): pure 1,8-diiodoperfluorooctane: δ -64.71 ($IC\mathit{F}_2CF_2CF_2CF_2)_2$, -113.01 ($ICF_2C\mathit{F}_2CF_2CF_2)_2$, -120.20

$(ICF_2CF_2CF_2CF_2)_2$, -121.05 $(ICF_2CF_2CF_2CF_2)_2$; co-crystal: $\Delta\delta_{(ICF2CF2CF2CF2)2}$ = 0.10, $\Delta\delta_{(ICF2CF2CF2CF2)2}$ = 0.01, $\Delta\delta_{(ICF2CF2CF2CF2)2}$ = 0.00, $\Delta\delta_{(ICF2CF2CF2CF2)2}$ = 0.00.

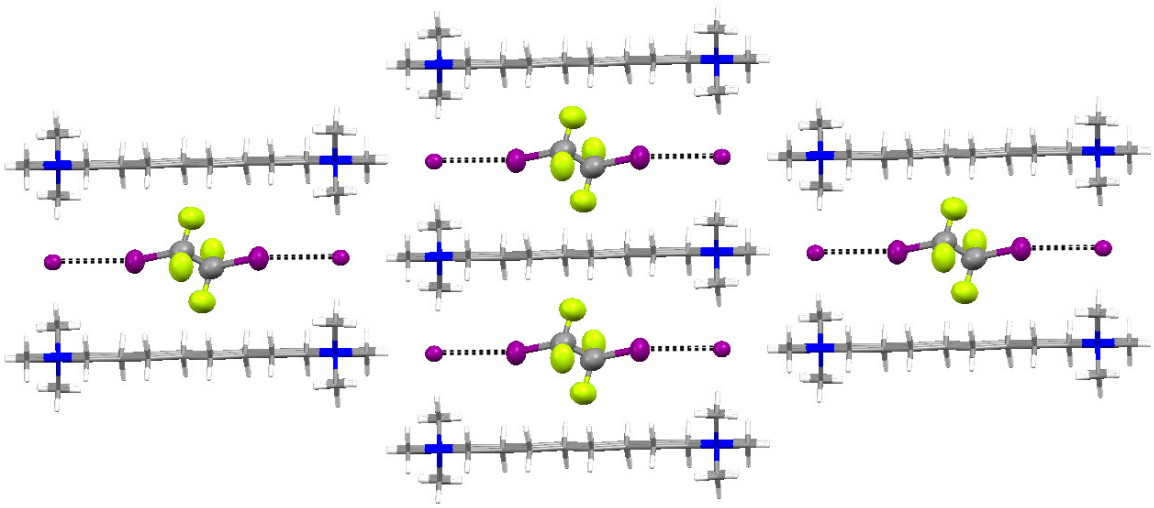

Fig. S1. The crystal packing of the matching complex **1a·2a** viewed down crystallographic *a* axis.

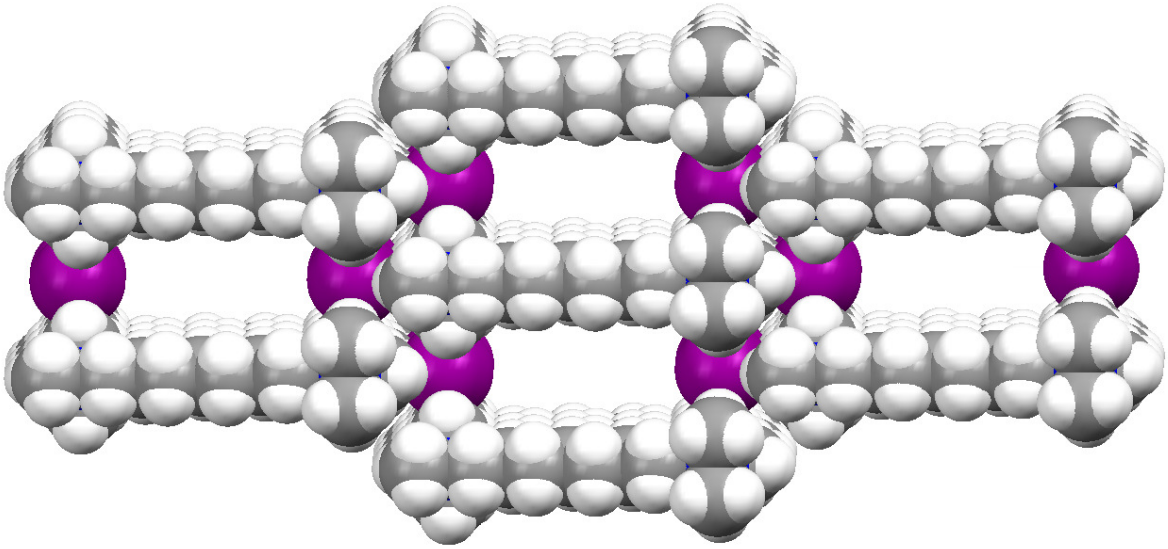

Fig. S2. The crystal packing of the complex **1a·2a** viewed down crystallographic *a* axis (same as above). The 1,2-diiodotetrafluoroethane molecules have been removed electronically to better show the formation of channels running along the crystallographic *a* axis. Removal of the diiodotetrafluoroethane molecules leaves a total potential solvent area volume accessible of 215.3 $Å^3$ per unit cell, corresponding to the 31.8% of the unit cell volume of the crystal (37.1% for **1b·2b**, 41.8% for **1c·2c**; calculated with PLATON).

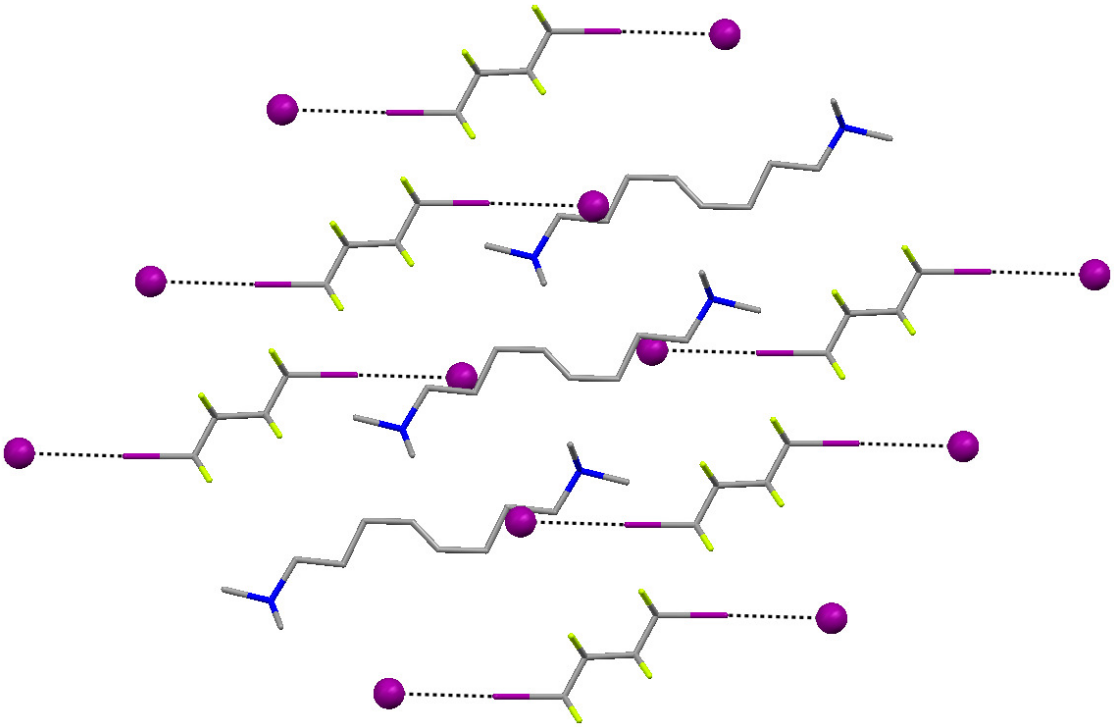

Fig. S3. The crystal packing of the mismatching complex **1a·2b** viewed down crystallographic *b* axis.

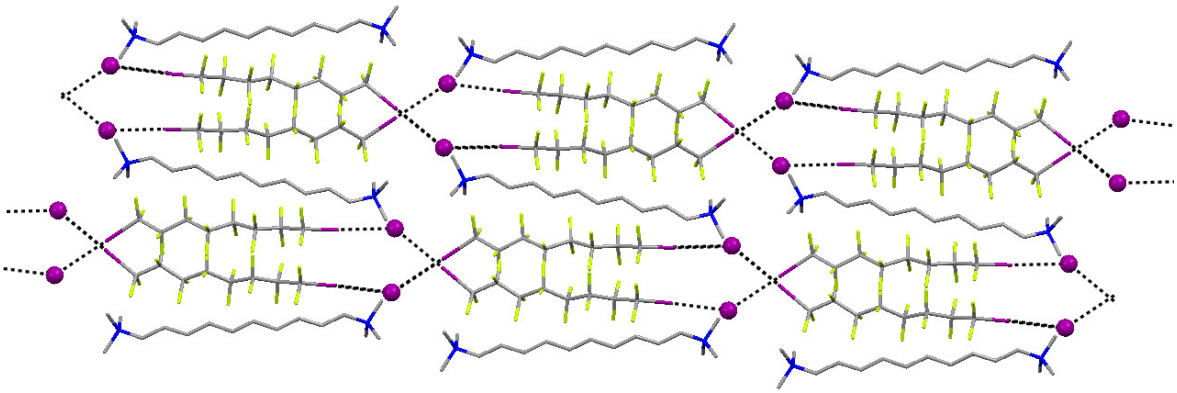

Fig. S4. The crystal packing of the mismatching complex **1b·2d** viewed down crystallographic *c* axis.

Table S1. Crystal data and structure refinement for **1b**.

Empirical formula	$(C_{16}H_{38}N_2)^{2+}.2(H_2O).2(I^-)$	
Formula weight	548.32	
Temperature	295(2) K	
Wavelength	0.71073 Å	
Crystal system	Triclinic	
Space group	P -1	
Unit cell dimensions	a = 8.534(2)Å	α = 80.00(2)
	b = 8.858(2) Å	β = 73.486(14)°
	c = 8.891(2) Å	γ = 71.754(16)°
Volume	609.3(2)Å^3	
Z	1	
Density (calculated)	1.494 Mg/m^3	
Absorption coefficient	2.589 mm^{-1}	
F(000)	274	
Crystal size	0.24 x 0.22 x 0.20 mm^3	
θ_{max} (θ_{full}) for data collection	30.24 (27.50)°	
Completeness to θ_{full}	99.8 %	
Index ranges	$-11 \le h \le 11$	
	$-12 \le k \le 12$	
	$-12 \le l \le 12$	
Collected reflections	10688	
R_{int}	0.0185	
Independent reflections	3438	
Absorption correction	none	
Restraints , parameters	2, 106	
Goodness-of-fit on F^2	1.086	
Final R indices [$I>2\sigma(I)$]	R_1 = 0.0229	wR_2 = 0.0619
Final R indices [all data]	R_1 = 0.0266	wR_2 = 0.0642
Largest diff. hole and peak	-0.34, 0.66 eA^{-3}.	

Table S2. Crystal data and structure refinement for **1a·2a**.

Empirical formula	$(C_{14}H_{34}N_2)^{2+}.(C_2F_4I_2).2(I^-)$	
Formula weight	838.05	
Temperature	253(2) K	
Wavelength	0.71073 Å	
Crystal system	Triclinic	
Space group	P -1	
Unit cell dimensions	a = 5.842(2) Å	α = 103.19(3)
	b = 7.648 (3) Å	β = 99.05(3)°
	c = 15.769 (6) Å	γ =90.05(3)°
Volume	676.3(4)Å^3	
Z	1	
Density (calculated)	2.058 Mg/m^3	
Absorption coefficient	4.639 mm^{-1}	
F(000)	392	
Crystal size	0.01 x 0.09 x 0.30 mm^3	
θ_{max} (θ_{full}) for data collection	24.83 (22.50)°	
Completeness to θ_{full}	99.8 %	
Index ranges	$-6 \le h \le 6$; $-8 \le k \le 9$	
	$-17 \le l \le 18$	
Collected reflections	4264	
R_{int}	0.0631	
Independent reflections	2037	
Absorption correction	Based on multi-scan	
Min. and max. transmission	0.337, 0.955	
Restraints , parameters	109, 133	
Goodness-of-fit on F^2	1.067	
Final R indices [$I>2\sigma(I)$]	R_1 = 0.0450	wR_2 = 0.1114
Final R indices [all data]	R_1 = 0.0604	wR_2 = 0.1196
Largest diff. hole and peak	-1.11, 1.61 eA^{-3}.	

Table S3. Crystal data and structure refinement for **1b·2b**.

Empirical formula	$(C_{16}H_{38}N_2)^{2+}.(C_4F_8I_2).2(I^-)$	
Formula weight	966.12	
Temperature	297(2) K	
Wavelength	0.71073 Å	
Crystal system	monoclinic	
Space group	*C*2/*m*	
Unit cell dimensions	a = 35.516(9) Å	α = 90.00 °
	b = 7.809 (2) Å	β = 98.52(2) °
	c = 5.9097 (16) Å	γ =90.00 °
Volume	1621.0(7) $Å^3$	
Z	2	
Density (calculated)	1.979 Mg/m^3	
Absorption coefficient	3.902 mm^{-1}	
F(000)	912	
Crystal size	0.04 x 0.18 x 0.19 mm^3	
θ_{max} (θ_{full}) for data collection	27.51 (27.51)°	
Completeness to θ_{full}	99.7 %	
Index ranges	$-45 \le h \le 44$; $-10 \le k \le 10$	
	$-7 \le l \le 7$	
Collected reflections	7760	
R_{int}	0.0292	
Independent reflections	2004	
Absorption correction	Based on multi-scan	
Min. and max. transmission	0.693, 1.000	
Restraints , parameters	18, 115	
Goodness-of-fit on F^2	1.067	
Final R indices [$I>2\sigma(I)$]	R_1 = 0.0402	wR_2 = 0.1085
Final R indices [all data]	R_1 = 0.0476	wR_2 = 0.1153
Largest diff. hole and peak	-0.78, 1.20 eA^{-3}.	

Table S4. Crystal data and structure refinement for **1c·2c**.

Empirical formula	$(C_{18}H_{42}N_2)^{2+}.(C_6F_{12}I_2).2(I^-)$	
Formula weight	1094.20	
Temperature	203(2) K	
Wavelength	0.71073 Å	
Crystal system	triclinic	
Space group	*P* -1	
Unit cell dimensions	a = 5.806(2) Å	α = 80.72(2) °
	b = 7.702 (3) Å	β = 83.53(2) °
	c = 20.768 (2) Å	γ =89.50(5) °
Volume	910.7(5) $Å^3$	
Z	1	
Density (calculated)	1.995 Mg/m^3	
Absorption coefficient	3.501 mm^{-1}	
F(000)	520	
Crystal size	0.01 x 0.28 x 0.40 mm^3	
θ_{max} (θ_{full}) for data collection	30.08 (28.50)°	
Completeness to θ_{full}	99.6 %	
Index ranges	$-8 \le h \le 8$; $-10 \le k \le 10$	
	$-29 \le l \le 29$	
Collected reflections	17367	
R_{int}	0.0431	
Independent reflections	5301	
Absorption correction	Based on multi-scan	
Min. and max. transmission	0.420, 0.966	
Restraints , parameters	0, 190	
Goodness-of-fit on F^2	1.067	
Final R indices [$I>2\sigma(I)$]	R_1 = 0.0491	wR_2 = 0.1362
Final R indices [all data]	R_1 = 0.0637	wR_2 = 0.1446
Largest diff. hole and peak	-1.75, 2.97 eA^{-3}.	

Table S5. Crystal data and structure refinement for **1a·2b**.

Empirical formula	$(C_{14}H_{34}N_2)^{2+}.(C_4F_8I_2).2(I^-)$	
Formula weight	938.07	
Temperature	297(2) K	
Wavelength	0.71073 Å	
Crystal system	monoclinic	
Space group	*C*2/*m*	
Unit cell dimensions	a = 13.587(3) Å	α = 90.00 °
	b = 8.421 (2) Å	β = 94.47(2) °
	c = 13.850 (3) Å	γ =90.00 °
Volume	1579.8(6) $Å^3$	
Z	2	
Density (calculated)	1.972 Mg/m^3	
Absorption coefficient	4.000 mm^{-1}	
F(000)	3400	
Crystal size	0.06 x 0.12 x 0.36 mm^3	
θ_{max} (θ_{full}) for data collection	18.69 (18.69)°	
Completeness to θ_{full}	99.9 %	
Index ranges	$-14 \le h \le 14$; $-8 \le k \le 8$; $-33 \le l \le 33$	
Collected reflections	18783	
R_{int}	0.0285	
Independent reflections	2170	
Absorption correction	Based on multi-scan	
Min. and max. transmission	0.673, 1.000	
Restraints , parameters	362, 325	
Goodness-of-fit on F^2	1.037	
Final R indices [$I>2\sigma(I)$]	R_1 = 0.0485	wR_2 = 0.1274
Final R indices [all data]	R_1 = 0.0526	wR_2 = 0.1322
Largest diff. hole and peak	-0.38, 0.680 eA^{-3}.	

Table S6. Crystal data and structure refinement for **1b·2d**.

Empirical formula	$(C_{16}H_{38}N_2)^{2+}.(C_8F_{16}I_2).2(I^-)$	
Formula weight	1820.04	
Temperature	296(2) K	
Wavelength	0.71073 Å	
Crystal system	orthorhombic	
Space group	*Aba*2	
Unit cell dimensions	a = 16.120(4) Å	α = 90.00 °
	b = 36.926(8) Å	β = 90.00 °
	c = 9.457 (2) Å	γ =90.00 °
Volume	5629(2) $Å^3$	
Z	4	
Density (calculated)	2.148 Mg/m^3	
Absorption coefficient	4.000 mm^{-1}	
F(000)	880	
Crystal size	0.06 x 0.19 x 0.30 mm^3	
θ_{max} (θ_{full}) for data collection	27.50 (27.50)°	
Completeness to θ_{full}	99.9 %	
Index ranges	$-8 \le h \le 8$; $-10 \le k \le 10$	
	$-29 \le l \le 29$	
Collected reflections	10164	
R_{int}	0.0200	
Independent reflections	1941	
Absorption correction	Based on multi-scan	
Min. and max. transmission	0.664, 1.000	
Restraints , parameters	60, 124	
Goodness-of-fit on F^2	1.067	
Final R indices [$I>2\sigma(I)$]	R_1 = 0.0283	wR_2 = 0.0706
Final R indices [all data]	R_1 = 0.0339	wR_2 = 0.0750
Largest diff. hole and peak	-0.60, 1.00 eA^{-3}.	

Gas-solid reaction between octamethonium iodide 1a and 1,2-diiodotetrafluoroethane 2a.

10 mg of octamethonium iodide **1a** and 300 mg of 1,2-diiodoperfluoroethane **2a** were introduced in two separated vials and put in a closed glass jar. The volatile **2a** was allowed to diffuse its vapors during 6h at ambient conditions. The resulting yellow solid was analyzed by PXRD and NMR (see Fig. S7). The 1:1 ratio of the two modules in co-crystal was proven by ^{1}H and ^{19}F NMR spectra in the presence of $(CF_3CH_2O)_2$ as an internal standard.

Gas-solid reaction between decamethonium iodide 1b and 1,4-diiodooctafluorobutane 2b.

20 mg of decamethonium iodide **1b** and 100 mg of 1,4-diiodooctafluorobutane **2b** were introduced in two separated vials and put in a closed glass jar. The volatile **2b** was allowed to diffuse its vapors during 7 days at ambient conditions. The resulting yellow solid was analyzed by PXRD and NMR (see Fig. S8). The 1:1 ratio of the two modules in co-crystal was proven by ^{1}H and ^{19}F NMR spectra in the presence of $(CF_3CH_2O)_2$ as an internal standard.

Gas-solid reaction between dodecamethonium iodide 1c and 1,6-diiodoperfluorohexane 2c.

10 mg of dodecamethonium iodide **1c** and 100 mg of 1,6-diiodoperfluorohexane **2c** were introduced in two separated vials and put in a closed glass jar. The volatile **2c** was allowed to diffuse its vapors during 3 days at 40 °C. The resulting white solid was analyzed by PXRD and NMR (see Fig. 2, A, B, and C, or S9). The 1:1 ratio of the two modules in the solid was proven by ^{1}H and ^{19}F NMR spectra in the presence of $(CF_3CH_2O)_2$ as an internal standard.

Powder X-ray diffraction results

Pure polymethylene bismethonium iodides **1a-d**

The measured and simulated powder X-ray diffraction (PXRD) patterns of pure decamethonium iodide **1b** can be seen in Fig. S5. The comparison of simulated and measured PXRD pattern confirms the structural uniformity of single crystal and the main component of bulk powder for **1b**. Furthermore, it seems to show additional weak phase, as the simulated and the experimental patterns for **1b** are not completely identical (some additional peaks can be seen, though being much weaker than the intensity gain of the main phase). This similar phase mixture is also observable from PXRD pattern taken from **1b·2b** complex after removal of DIPFA **2b** (see Fig. S16). Based on TG measurements, and the fact that the PXRD from a removal test of DIPFA is identical with a pattern of pure decamethonium congener **1b**, it suggested that the bulk powder of **1b** is mixture of anhydrous and dihydrate forms, which both capture selectively and quantitatively the matching DIPFA 1**b**. In case of the "emptied" complex, thus have been turned to anhydrous **1b,** hydrates partly while the sample is once again exposed to an ambient lab condition resulting phase mixture of both anhydrous and dihydrate forms.

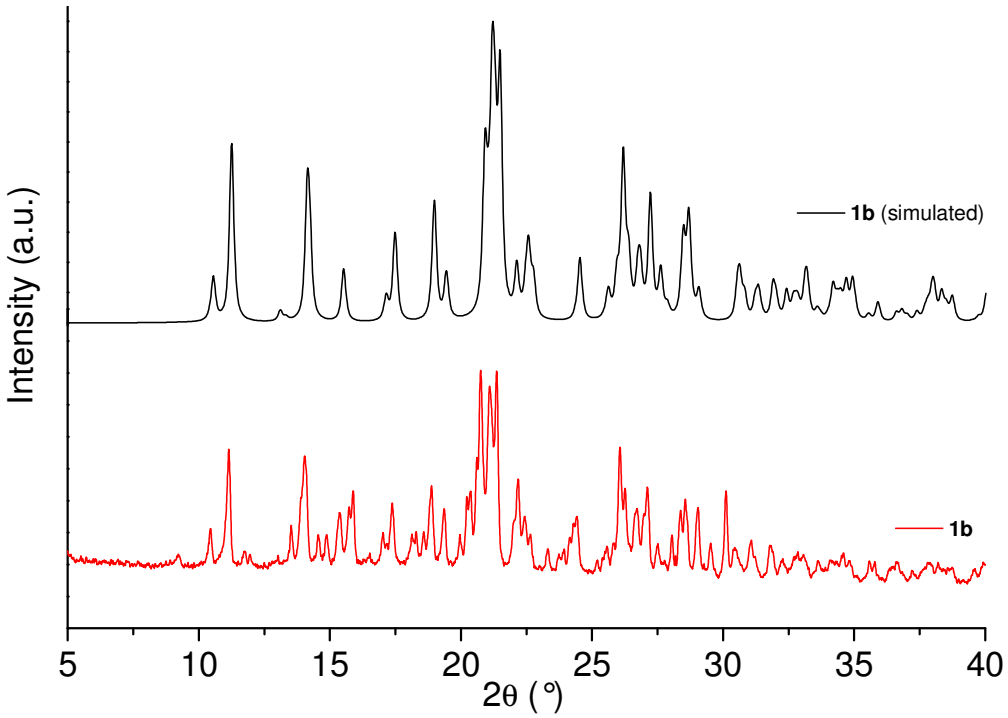

Fig. S5. Simulated and measured PXRD patterns of congener **1b**.

In case of congeners **1a**, **1c** and **1d** comparison cannot be made, as single crystal data was unavailable for these bismethonium congeners due to poor quality of single crystals

obtained for structure determination. Therefore only the measured PXRD patterns are presented in Fig. S6. Based on the overall intensity gains of the patterns (examined in counts/ s) and peak widths of the diffraction peaks, the bismethonium iodides **1a-1c** possess rather similar degree of crystallinity, whereas the **1d** is clearly less crystalline.

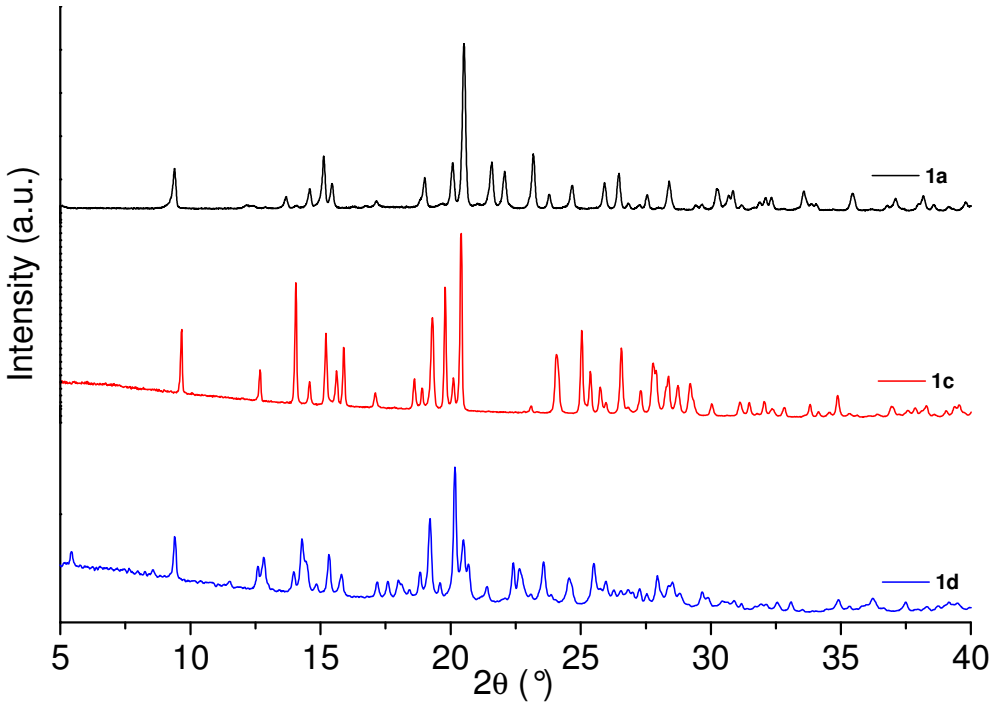

Fig. S6. Measured PXRD patterns of **1a**, **1c** and **1d**.

Matching complexes

The comparisons between the simulated and measured PXRD patterns of matching complexes **1a·2a**, **1b·2b**, and **1c·2c** obtained from solution and gas-solid reaction, are shown in Figures S7-S9, respectively. In case of the complex **1d·2d**, the successful formation of adduct was examined by comparing diffraction data of the **1d·2d** (obtained from solution) and pure bismethonium iodide **1d** (Fig. S10)**,** because the single crystal data for this adduct was unavailable. All three complexes **1a-c·2a-c** are clearly in the same structural form that were found for single crystal analogues, regardless of either they were prepared via solution or gas-solid reaction path. In case of **1d·2d**, diffraction peaks originating from the tetradecamethonium iodide **1d** were not observed in the PXRD pattern of the complex, supporting assumption that the complex formation was occurred quantitatively. Furthermore, the impression of pattern of **1d·2d** resembles clearly of those measured for the other matching complexes, which in part strengthen the statement due the fact all the matching complexes possess similarities in peak positions of strongest peaks and general grouping of the peaks (see PXRD patterns of **1a·2a** and **1b·2b,** for example). The crystallinity of the complexes **1a-d·2a-d** follows the trend that was found already for the pure iodides **1a**-**d**. The complexes **1a-c·2a-c** are clearly crystalline, and the **1d·2d** shows somewhat lower crystallinity.

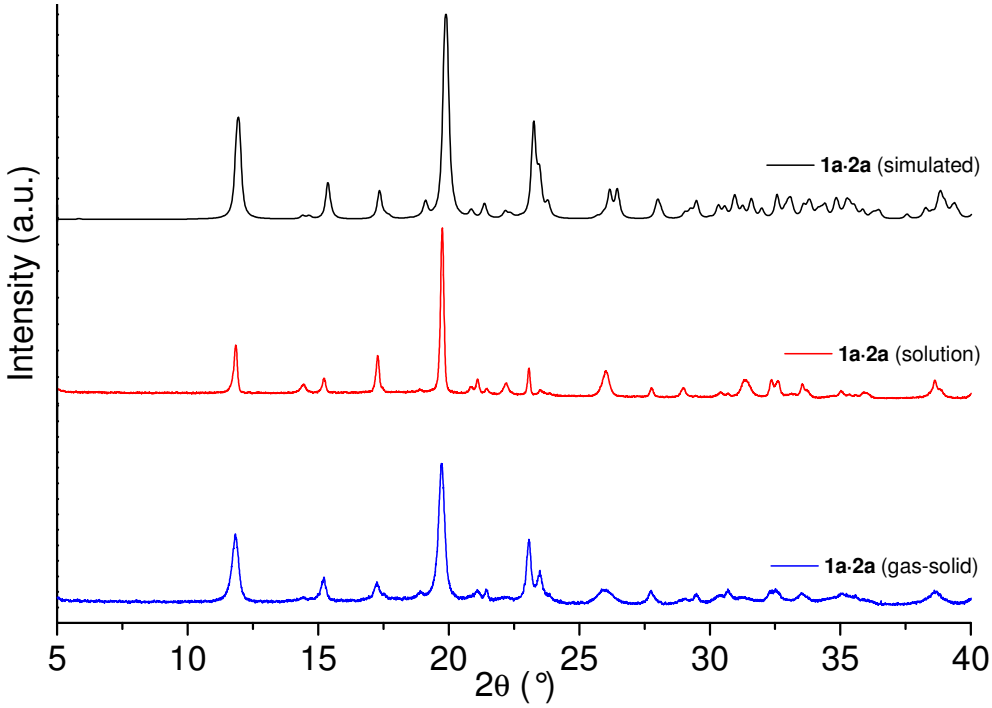

Fig. S7. Simulated and measured PXRD patterns of **1a·2a** obtained from solution and gas-solid reaction.

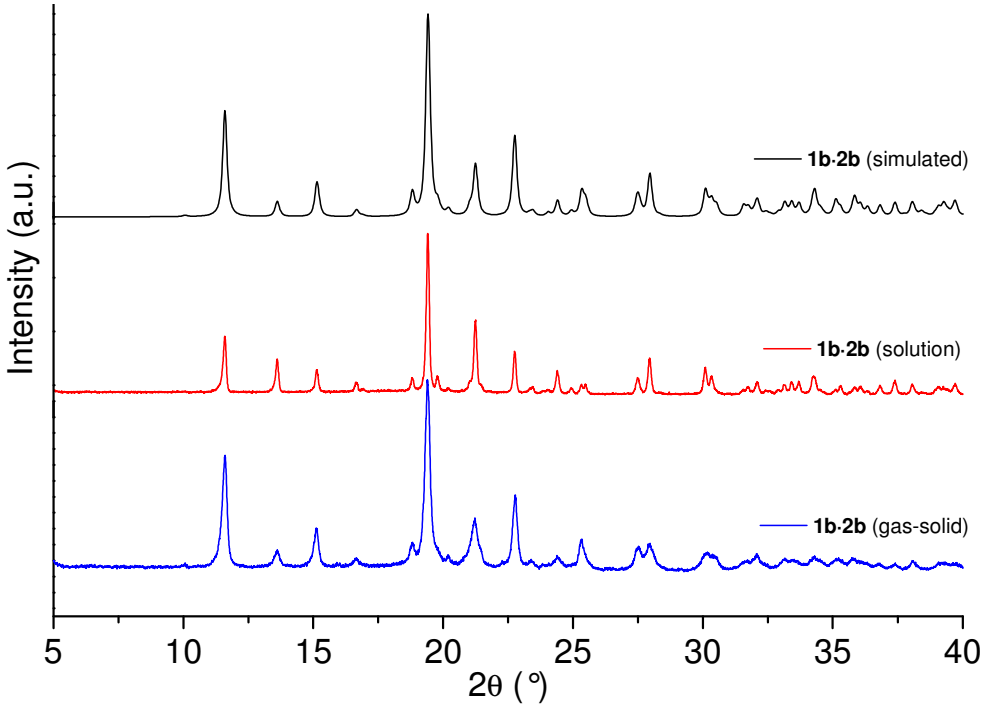

Fig. S8. Simulated and measured PXRD patterns of **1b·2b** obtained from solution and gas-solid reaction.

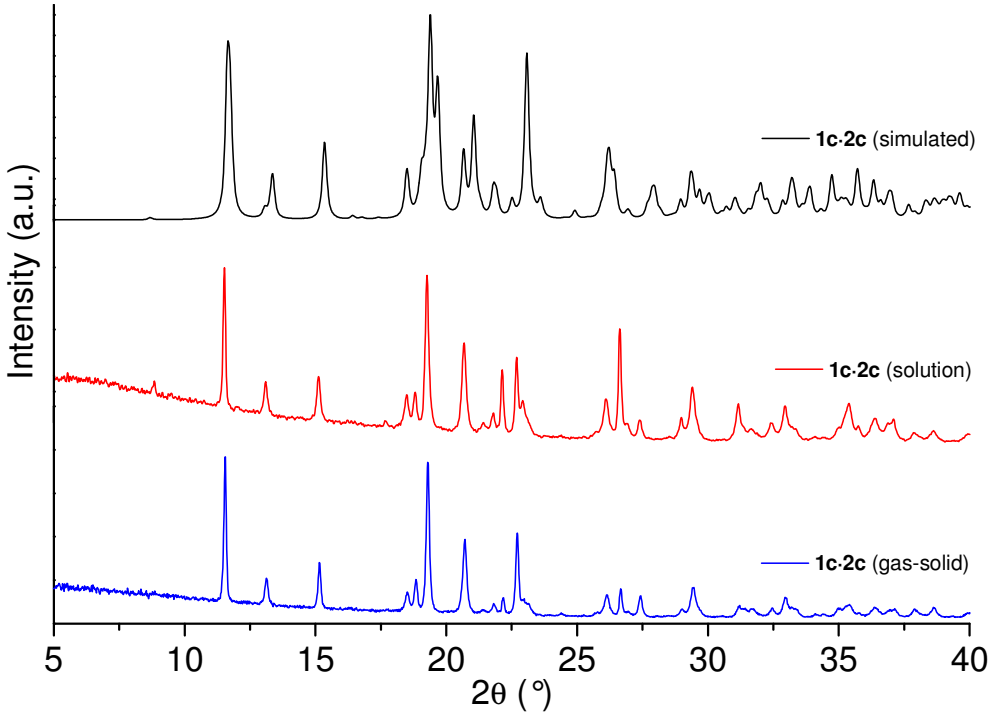

Fig. S9. Simulated and measured PXRD patterns of **1c·2c** obtained from solution and gas-solid reaction.

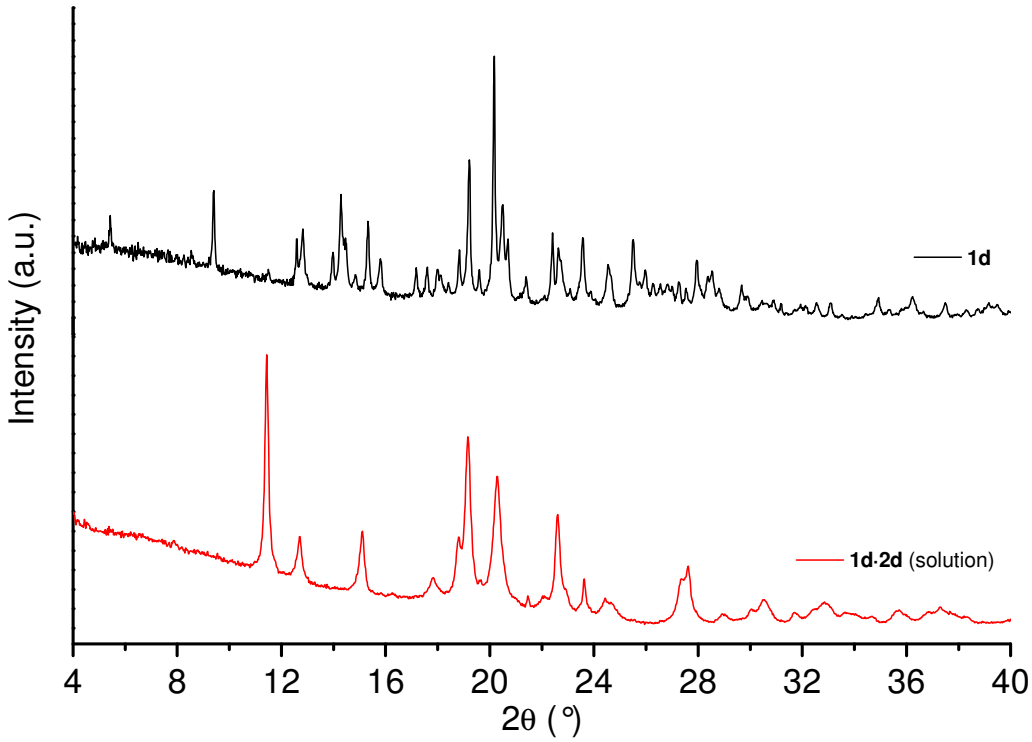

Fig. S10. Measured PXRD patterns of **1d** and **1d·2d** obtained from solution.

Mismatching complexes

The comparisons between the simulated and measured PXRD patterns of mismatching complexes **1a·2b** and **1b·2d,** obtained from a solution, are shown in Figures S11 and S12. In case of the complex **1a·2b** the bulk powder is structurally similar to its single crystal analogue, as nearly perfect match between the simulated and experimental patterns can be seen in Fig. S11. Somewhat different observation can be made for **1b·2d** as the PXRD pattern indicates presence of a phase mixture, which consist mainly of the expected complex and in minor fraction the decamethonium iodide **1b** (Fig. S12).

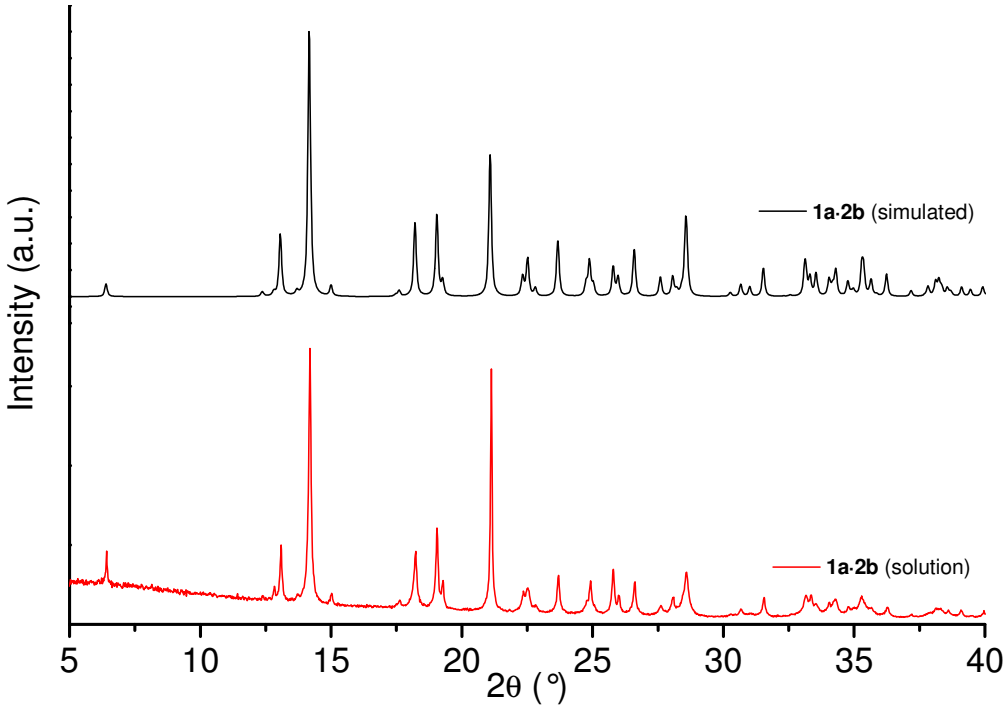

Fig. S11. Simulated and measured PXRD patterns of mismatching complex **1a·2b** obtained from a solution.

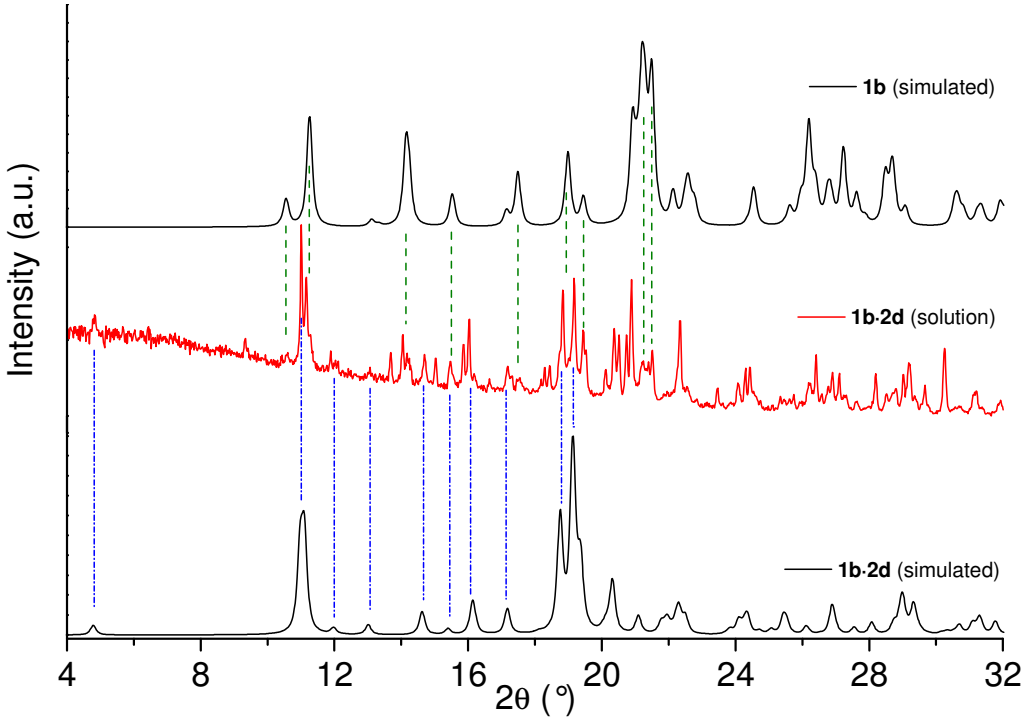

Fig. S12. Simulated and measured PXRD patterns of mismatching complex **1b·2d** and simulated pattern of decamethonium iodide **1b.**

Rietveld analysis

In addition to a visual inspection of the PXRD patterns, the Rietveld analyses were made for certain complexes to evaluate the lattice parameters of complexes also in powder state. The lattice parameters for complexes **1c·2c** and **1a·2b** are presented in Table S7. The final Rietveld refinement plot corresponding to **1c·2c** is exemplified in Fig. S13. The Rietveld refinements converged nicely (weighted R-factors <10%) ending up to lattice parameters, which were similar to that of found on corresponding single crystals. The preparation methods for yielding bulk powders did not influenced to the lattice parameters, as the obtained structural parameters remained similar regardless of the preparation route.

Table S7. Cell parameters determined both from powder and single crystal data for matching complex **1c·2c** and mismatching complex **1a·2b**

Comp.	**1c·2c**			**1a·2b**	
Param.	(PXRD)[a]	(PXRD)[b]	(SC)	(PXRD)[a]	(SC)
a	5.9150(5)	5.9157(4)	5.806(2)	13.589(1)	13.587(3)
b	7.8418(7)	7.8465(5)	7.702(3)	8.4167(7)	8.421(2)
c	20.609(1)	20.610(1)	20.768(6)	13.868(1)	13.850(3)
α	79.321(6)	79.306(5)	80.72(2)	90	90
β	82.794(5)	82.796(4)	83.53(2)	94.419(6)	94.47(2)
γ	90.013(9)	90.026(7)	89.50(2)	90	90
V	931.70	932.35	910.665	1581.40	1579.84
SG	P-1	P-1	P-1	C 1 2/m 1	C 1 2/m 1
Temp (K)	295(2)	295(2)	203(2)	295(2)	297(2)
R_p (%)	5.90	6.71		7.86	
R_{wp} (%)	7.81	8.63		10.09	

SC = single crystal data; a = from solution; b = from gas-solid reaction.

$$R_B = 100\frac{\sum_{\mathbf{h}}\left|{}^{\mathrm{I}}I_{obs,\mathbf{h}}{}^{\mathrm{I}} - I_{calc,\mathbf{h}}\right|}{\sum_{\mathbf{h}}\left|{}^{\mathrm{I}}I_{obs,\mathbf{h}}{}^{\mathrm{I}}\right|} \qquad R_{wp} = 100\left[\frac{\sum_{i=1,n} w_i\left|y_i - y_{c,i}\right|^2}{\sum_{i=1,n} w_i y_i^2}\right]^{1/2}$$

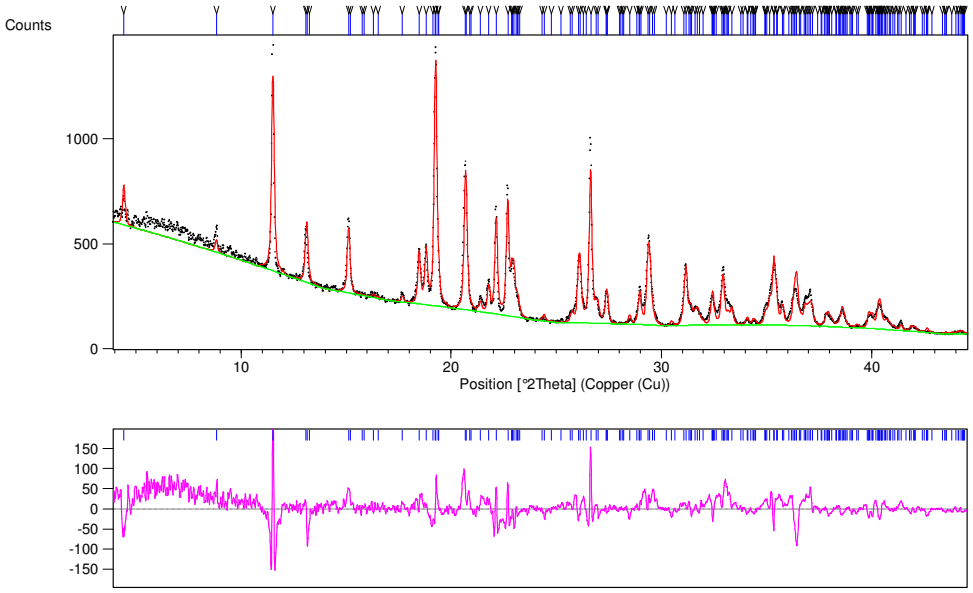

Fig. S13. Rietveld refinement plot of **1c·2c** Blue tick marks represent the peak positions, black dots the experimental powder data, the red line a calculated profile and the green line background profile. The pink line in lower graph represents the difference plot between calculated and the experimental powder profile.

Gas-solid reaction of the solid complex 1a·2b with vapors of 1,2-diiodotetrafluoroethane 2a.
The complex **1a·2b** was obtained via the standard procedure of crystallization from solution. The finely ground solid **1a·2b** and liquid 1,2-diiodotetrafluoroethane **2a** were introduced in two separated vials and placed in a closed glass jar. The 1,2-diiodotetrafluoroethane **2a** was allowed to diffuse its vapors during 7 days at ambient conditions. By PXRD we observed a complete replacement of 1,4-diiodoperfluorobutane by 1,2-diiodoperfluoroethane in the complex (see Fig. 2, F and G, or S14). The ratio HC/PFC is 1/1, as determined by NMR.

Gas-solid reaction of the solid complex 1a·2a with vapors of 1,4-diiodooctafluorobutane 2b.
The complex **1a·2a** was obtained via the standard procedure of crystallization from solution. The finely ground solid **1a·2a** and liquid 1,4-diiodooctafluorobutane **2b** were introduced in two separated vials and placed in a closed glass jar. The 1,4-diiodooctafluorobutane **2b** was allowed to diffuse its vapors during 7 days at ambient conditions. The resulting solid was analyzed by PXRD. No change of the crystal phase of the complex **1a·2a** was observed (see Fig. 2, D and E, or S14).

The selectivity of the matching complexes was demonstrated by the guest-exchange reactions using the matching and mismatching complexes of **1a·2a** and **1a·2b**. The PXRD patterns measured after the complexes were exposed to DIPFAs **2b** (former) and to **2a** (latter)**,** are presented in Fig. S14. The patterns which were obtained after exposure of DIPFAs clearly demonstrate the selectivity properties of the system, as both patterns correspond to the simulated pattern of complex **1a·2a**. In case of **1a·2b,** the replacement of **2b** to **2a** is occurred completely, whereas in case of **1a·2a** replacement is not occurred from **2a** to **2b** at all.

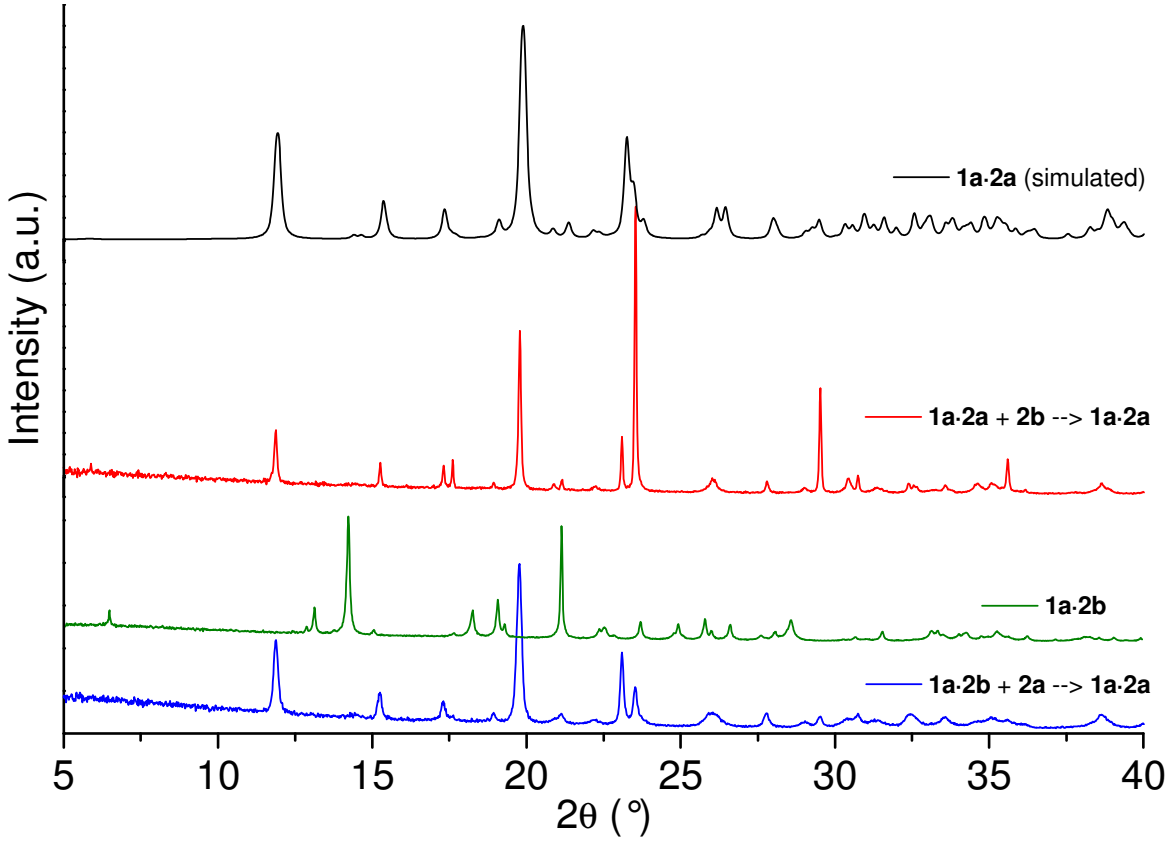

Fig. S14. Simulated PXRD pattern of complex **1a·2a** and measured patterns of **1a·2a** after exposure to DIPFA **2b** (red), and **1a·2b** before (green) and after (blue) exposure to **2a**.

Precipitation of the 1d·2d complex formed by tetradecamethonium iodide and 1,8-diiodoperfluorooctane from a solution of mixture of DIPFAs of industrial origin.
47 mg of a distillation residue coming from a typical industrial process and having the following composition: 1,8-diiodoperfluorooctane **2d** (24.2%), 1,10-diiodoperfluorodecane **2e** (41.9%), 1,12-diiodoperfluorododecane **2f** (23.0%), 1,14-diiodoperfluorotetradecane (8.3%) and 1,16-diiodoperfluorohexadecane (2.6%) were dissolved in CCl_4. This solution was added of a CH_3OH solution containing 9 mg of tetradecamethonium iodide **1d** (1 eq for 1 eq of **2d** in the mixture). Almost immediately, a white solid precipitated, which was washed with fresh CCl_4 and analyzed by GC, NMR, and melting point.

Precipitation of the 1e·2e complex formed by hexadecamethonium iodide and 1,10-diiodoperfluorodecane from a solution of mixture of DIPFAs of industrial origin.
25 mg of a distillation residue coming from a typical industrial process and having the following composition: 1,8-diiodoperfluorooctane **2d** (24.2%), 1,10-diiodoperfluorodecane **2e** (41.9%), 1,12-diiodoperfluorododecane **2f** (23.0%), 1,14-diiodoperfluorotetradecane (8.3%) and 1,16-diiodoperfluorohexadecane (2.6%) were dissolved in CCl_4. This solution was added of a CH_3OH solution containing 6 mg of hexadecamethonium iodide **1e** (1 eq for 1 eq of **2e** in the mixture). Almost immediately, a white solid precipitated, which was washed with fresh CCl_4 and analyzed by GC, NMR, and melting point.

Precipitation of the 1f·2f complex formed by octadecamethonium iodide and 1,12-diiodoperfluorododecane from a solution of a mixture of of industrial origin.
68 mg of a distillation residue coming from a typical industrial process and having the following composition: 1,8-diiodoperfluorooctane **2d** (24.2%), 1,10-diiodoperfluorodecane **2e** (41.9%), 1,12-diiodoperfluorododecane **2f** (23.0%), 1,14-diiodoperfluorotetradecane (8.3%) and 1,16-diiodoperfluorohexadecane (2.6%) were dissolved in CCl_4. This solution was added of a CH_3CN solution containing 10 mg of octadecamethonium iodide **1f** (1 eq for 1 eq of **2f** in the mixture). Immediately, a white solid precipitated, which was washed with fresh CCl_4 and analyzed by GC, IR, NMR, and melting point.

Complex 1e·2e formed by hexadecamethonium iodide and 1,10-diiodoperfluorodecane.
White solid, m.p. 222°C. ^{19}F NMR (470.6 MHz, CD_3OD, 0.002 M): δ -62.48 ($IC\mathit{F}_2CF_2CF_2CF_2CF_2)_2$, -114.37 ($ICF_2CF_2C\mathit{F}_2CF_2CF_2)_2$, -121.84 ($ICF_2CF_2CF_2C\mathit{F}_2CF_2)_2$, -122.66 ($ICF_2CF_2CF_2CF_2C\mathit{F}_2)_2$.

Complex 1f·2f formed by octadecamethonium iodide and 1,12-diiodoperfluorododecane.
White solid, m.p. 210°C. I.R. (cm^{-1}, selected bands): 3010, 2933, 2863, 1475, 1216, 1151, 1146, 1101, 1061, 957, 908, 730. ^{19}F NMR (470.6 MHz, CD_3OD, 0.002 M): δ -66.75 ($IC\mathit{F}_2CF_2CF_2CF_2CF_2CF_2)_2$, -115.24 ($ICF_2C\mathit{F}_2CF_2CF_2CF_2CF_2)_2$, -122.29 ($ICF_2CF_2C\mathit{F}_2CF_2CF_2CF_2)_2$, -123.11 ($ICF_2CF_2CF_2C\mathit{F}_2C\mathit{F}_2C\mathit{F}_2)_2$.

Gas phase IR experiments on the complex 1a·2a

The complex octamethonium iodide/1,2-diiodoperfluoroethane **1a·2a** was closed at ambient pressure in a sealed heating cell. Vapour phase IR spectra were registered each 10°C between 50 and 190°C. Absorption bands characteristic of the DIPFA **2a** were observed at 709, 839, 979 and 1115 cm^{-1}. Massive release of **2a** started at 165 °C (the boiling point of pure **2a** is 112 °C), with the maximum release occurring at 185 °C, well before the melting temperature of the complex (201 °C).

Removal of 1,2-diiodoperfluoroethane 2a from the complex 1a·2a.

2 mg of finely ground complex octamethonium iodide/1,2-diiodoperfluoroethane **1a·2a** were put over a glass slide and heated at 190 °C with a hot plate. After 30 min a white solid was recovered, which showed a melting point of 266 °C, corresponding to the pure octamethonium iodide **1a** (confirmed by ^{19}F and ^{1}H NMR). I.R. (cm^{-1}, selected bands): starting **1a**: 3482, 3429, 3007, 2945, 2923, 2861, 1622, 1490, 1478, 1418, 966, 956, 910, 766, 733; **1a** after treatment: 3010, 2928, 2857, 1476, 1465, 1444, 1401, 1237, 965, 955, 921, 908, 870, 721. UATR-FT-IR confirmed that starting octamethonium iodide **1a** was in the hydrated form (mp: 270 °C), while from the above described treatment it was recovered in the dehydrated form.

Removal of 1,4-diiodoperfluorobutane 2b from the complex 1b·2b.

2 mg of finely ground complex decamethonium iodide/1,4-diiodoperfluorobutane **1b·2b** were put over a glass slide and heated at 210 °C with a hot plate. After 30 min a white solid was recovered, which showed a melting point of 247 °C, corresponding to the pure decamethonium iodide **1b** (confirmed by ^{19}F and ^{1}H NMR). I.R. (cm^{-1}, selected bands): starting **1b**: 3484, 3432, 3004, 2923, 2858, 1628, 1492, 1479, 964, 910, 731, 714; **1b** after treatment: 3005, 2920, 2852, 1491, 1478, 965, 908, 725. UATR-FT-IR confirmed that starting decamethonium iodide **1b** was in the hydrated form (mp: 250 °C), while from the above described treatment it was recovered in the dehydrated form.

Removal of 1,6-diiodoperfluorohexane 2c from the complex 1c·2c.

2 mg of finely ground complex dodecamethonium iodide/1,6-diiodoperfluorohexane **1c·2c** were put over a glass slide and heated at 200 °C with a hot plate. After 10 min a white solid was recovered, which showed a melting point of 229 °C, corresponding to the pure dodecamethonium iodide **1c** (confirmed by ^{19}F and ^{1}H NMR). I.R. (cm^{-1}, selected bands): starting **1c**: 3002, 2914, 2851, 1483, 1463, 1418, 1263, 972, 939, 916, 879, 731; **1c** after treatment: 3003, 2914, 2852, 1483, 1464, 1418, 1263, 973, 939, 917, 879, 731. UATR-FT-IR confirmed that starting dodecamethonium iodide **1c** was in the dehydrated form, as well as was the solid recovered from the above described treatment.

The complete removal of **2a-d** is witnessed by the PXRD pattern measured from the heat treated sample, as complexes **1a-d·2a-d** have transformed completely back to decamethonium congeners **1a-d** (Figures S15-18). Similar removal tests were made also by TG in more quantitative method; see following chapters.

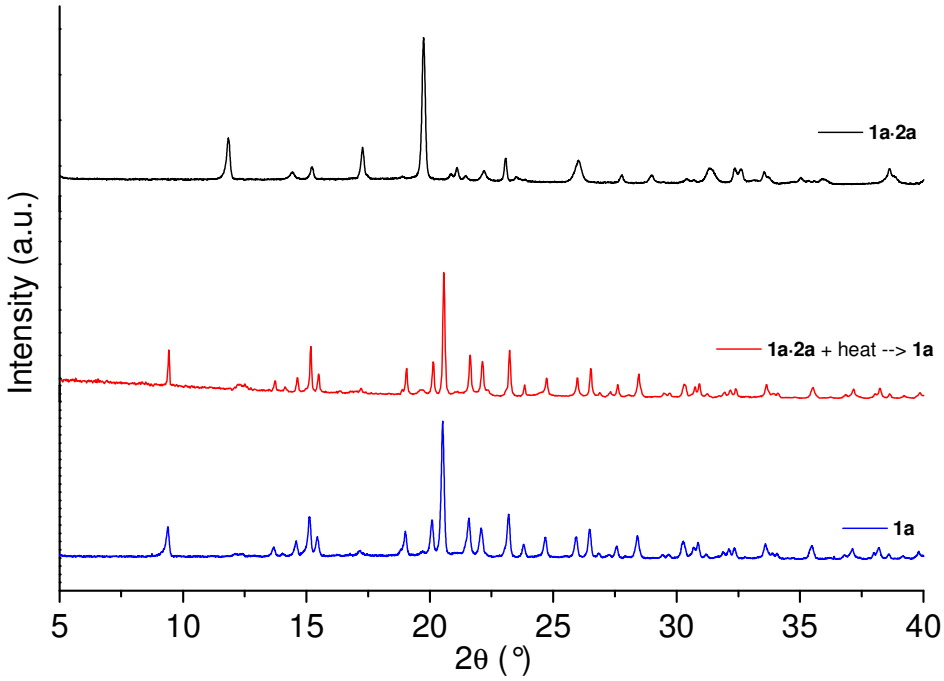

Fig. S15. Experimental PXRD patterns of **1a** and **1a·2a** measured before (top) and after (middle) heat treatment.

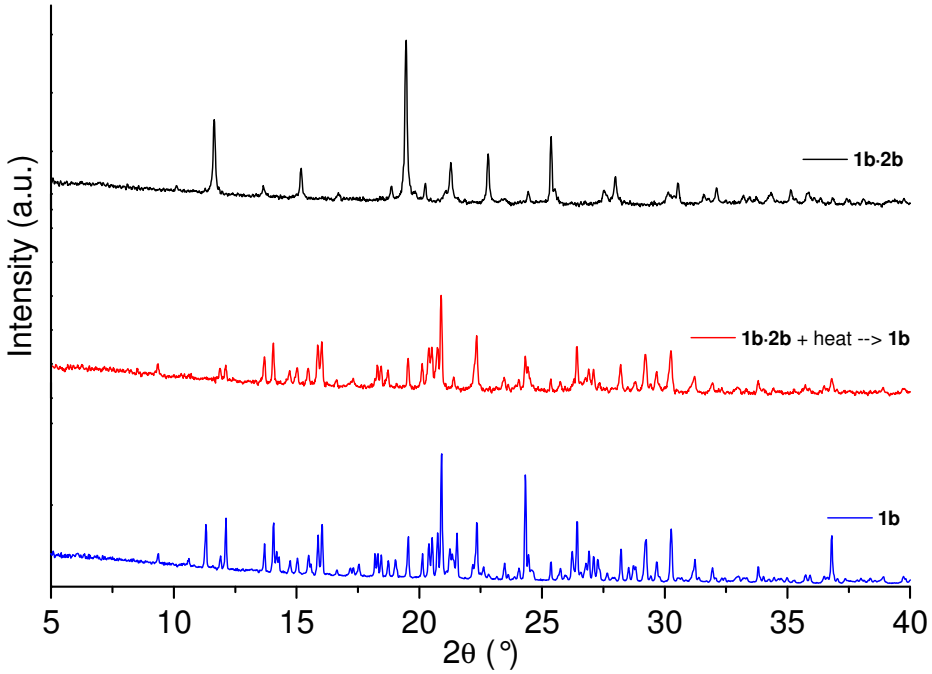

Fig. S16. Experimental PXRD patterns of **1b** and **1b·2b** measured before and after heat treatment.

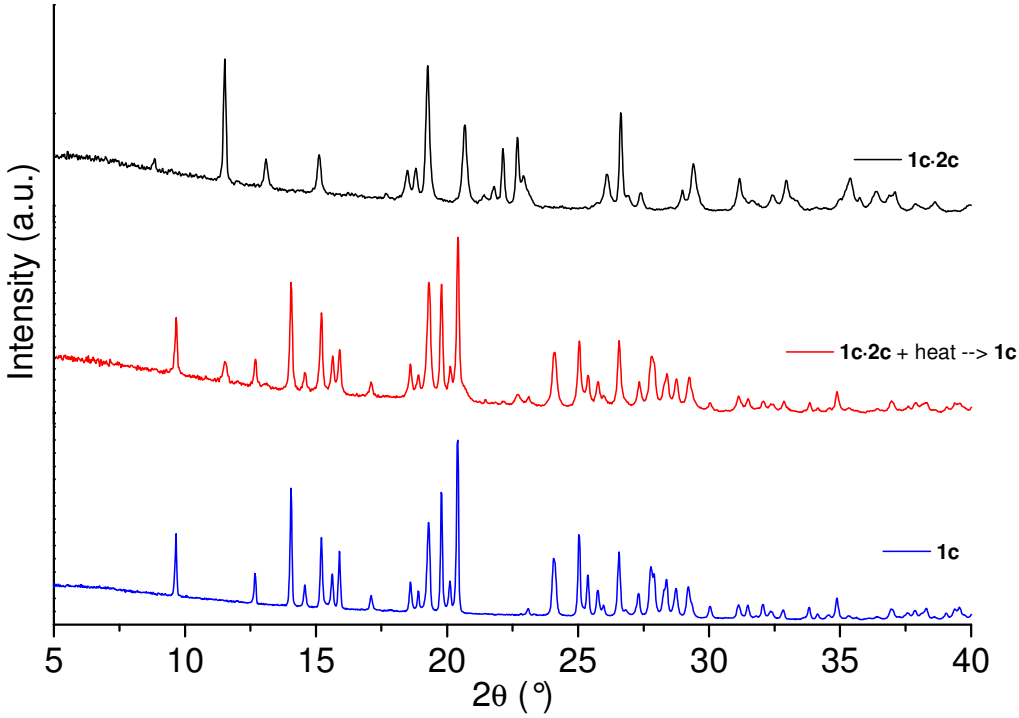

Fig. S17. Experimental PXRD pattern of **1c** and **1c·2c** measured before and after heat treatment.

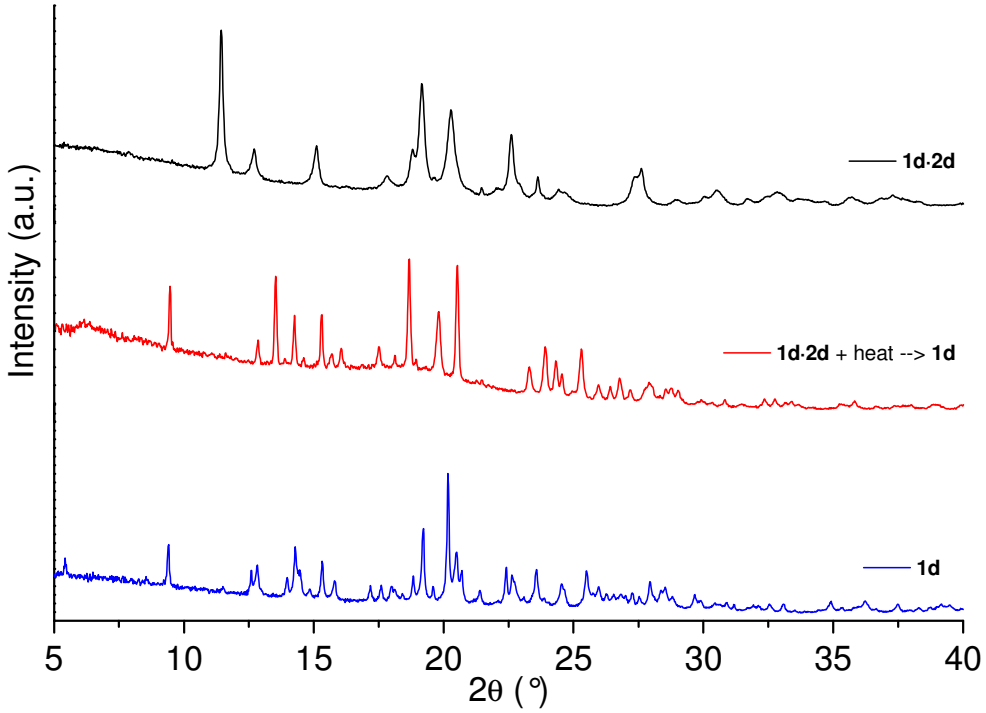

Fig. S18. Simulated PXRD pattern of **1d** and experimental patterns of **1d·2d** measured before and after heat treatment.

Thermal analysis results

Thermal properties of the complexes **1a-d·2a-d** were examined by means of thermogravimetry (TG) and differential scanning calorimetry (DSC). The DSC was used to monitor the thermal transitions on complexes while heated up to their melting points. The removal of DIPFAs from a complexes and decomposition temperature onsets on bismethonium congeners were examined by TG.

Thermogravimetry

The TG curves for bismethonium congeners **1a-d** are presented in Fig. S19 and the results are gathered in Table S8. All bismethonium iodides, except **1d** show similar decomposition temperature onsets varying from 258-265 °C. For **1d** somewhat lower decomposition onset was observed at 246°C. In addition the congener **1b** is in hydrated form as additional weight loss due to dehydration can be observed from 47 to 97 °C. The 3.2% Δwt-% (theor. for dihydrate 6.57%) corresponds roughly to a half of the theoretical ratio of dihydrated congener **1b** found by structure determination. This is explained by the presence of phase mixture of anhydrous and dihydrate forms in 1:1 ratio (See powder diffraction results).

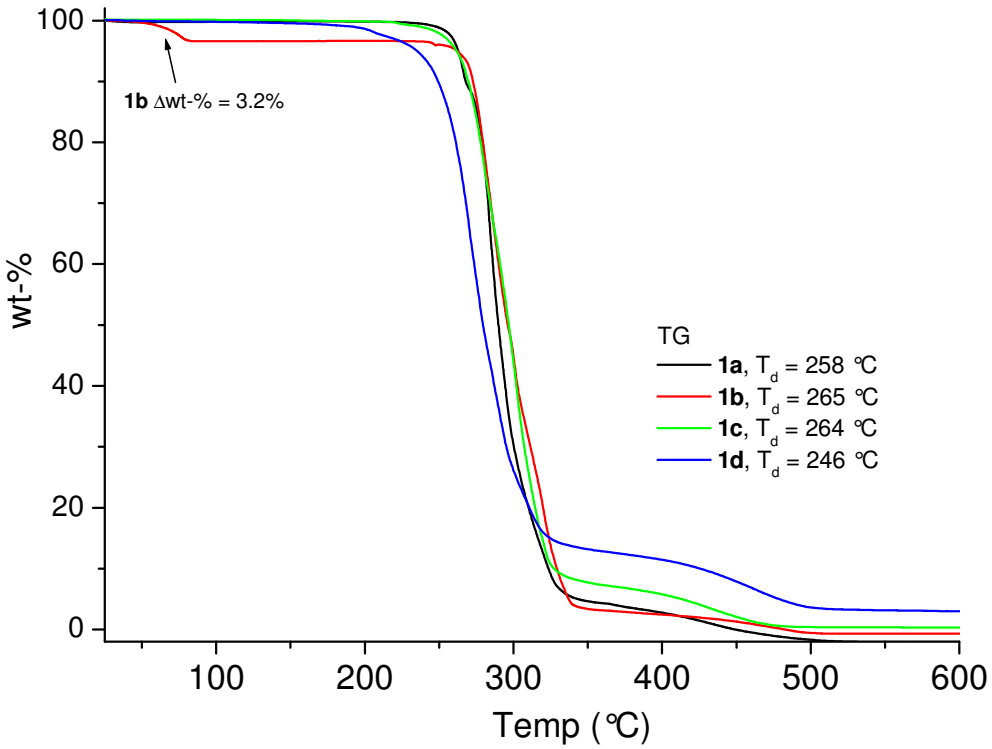

Fig. S19. TG curves of decamethonium congeners **1a-1d** measured at a heat rate of 10 °C/min under flowing air atmosphere. T_d = decomposition temperature onset.

Table S8. Melting points and decomposition temperature onsets for bismethonium congeners **1a-d**

Conge.	FW (g/ mol[1])	T_m (°C)	T_d (°C)
1a	484.25	201	258
1b	548.32	250	265
1c	540.36	222	264
1d	568.41	207	246

T_m = melting point, T_d = decomposition onset temperature

The TG analyses of matching complexes **1a-d·2a-d** revealed the complete removal of the DIPFA before the melting transition of the remaining "emptied" complex skeleton, as can be seen in Figures S20-26. Mainly, the samples prepared from solution have been examined but for certain complexes, samples prepared by gas-solid reaction were measured also. The complete removal of DIPFAs was observed again also on these samples (Figures S21 and S23). In addition, TG runs were made by adding an isothermal step (190 °C [175 °C for **1d·2d**] for 60 min) to nominal heat rate of 10 °C/min. The highly consistent results from all these measurements are gathered in to Table S9. The TG runs including the isothermal step, show the quantitative removal of DIPFAs on all four complexes, as >95% of DIPFAs have been evaporated already at the isothermal step, which is still clearly below the melting point of the "emptied" complex and/or the corresponding pure decamethonium congener. For **1a-d·2a-d** lower isothermal temperature was used due to somewhat lower decomposition temperature of the **1d** but still complete removal was observed.

Table S9. Observed and calculated weight losses of DIPFAs removed from matching complexes **1a-d·2a-d**

Comp.	FW (g/mol)	Δwt_{obs} (%)	Δwt_{calc} (%)	T_{end} (°C)	T_m (°C)	β (°C/min)
1a·2a	838.05	37.7	42.22 (**2a**)	191	201	10
1a·2a *		41.7	42.22 (**2a**)	190		10/ isotherm
1b·2b	966.12	47.0	46.97 (**2b**)	220	230	10
1b·2b *		44.6	46.97 (**2b**)	190		10/ isotherm
1c·2c	1094.20	50.5	50.62 (**2c**)	195	227	2
1c·2c *		49.8	50.62 (**2c**)	190		10/ isotherm
1d·2d	1222.28	53.1	53.47 (**2d**)	213	231	2
1d·2d **		52.4	53.47 (**2d**)	213		10/ isotherm

Δwt_{obs} = observed weight loss of leaving group, Δwt_{calc} = theoretical weight loss of leaving group, T_{end} = observed end temperature of DIPFA removal, T_m = melting point of the emptied complex, β = heating rate; TG run includes isothermal step at * = 190 °C or ** = 175 °C for 60 min.

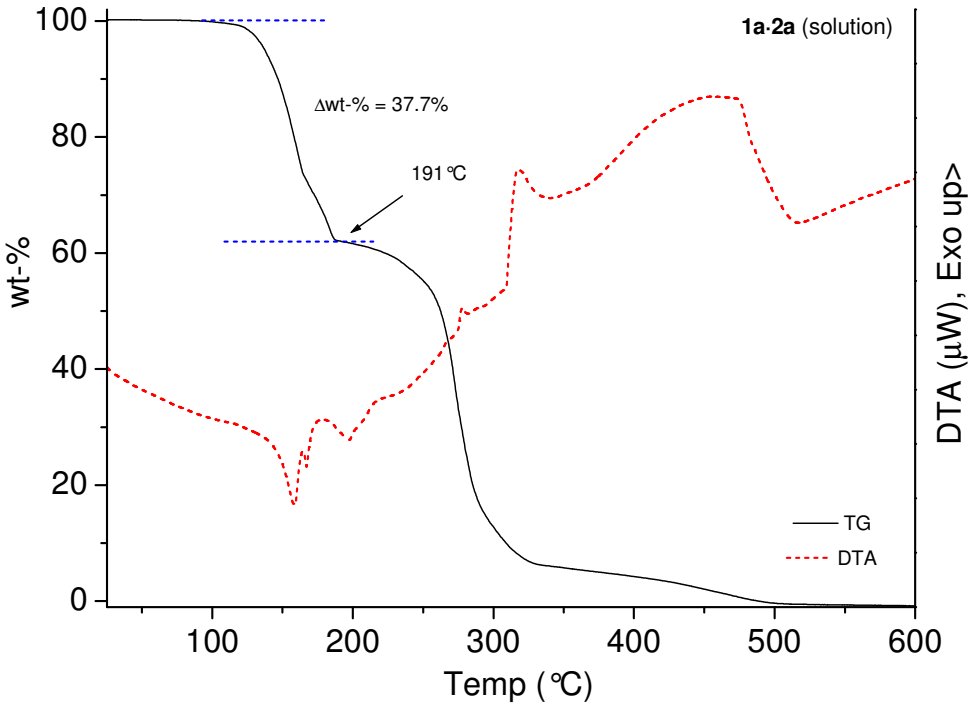

Fig. S20. TG and DTA curves of **1a·2a** obtained from solution.

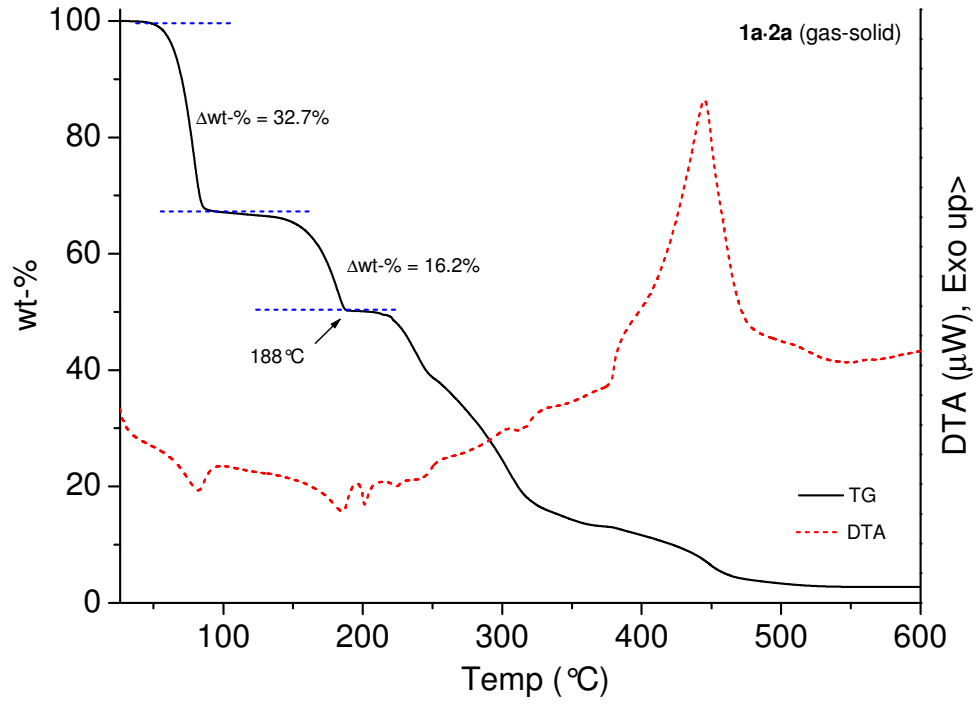

Fig. S21. TG and DTA curves of **1a·2a** obtained from gas-solid reaction (heat rate 10 °C/min).

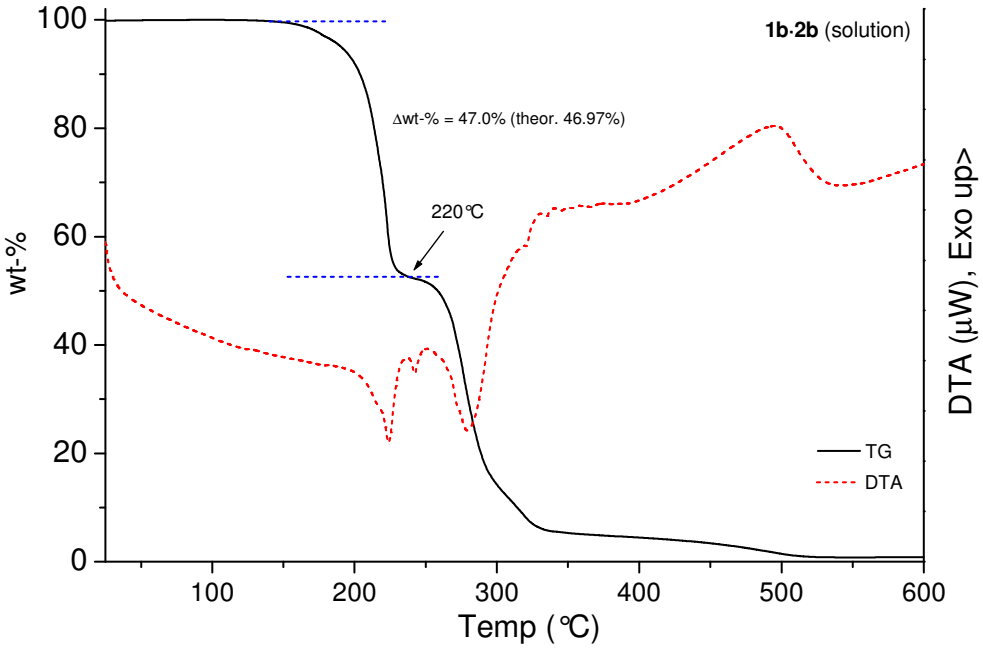

Fig. S22. TG and DTA curves of **1b·2b** obtained from solution (heat rate 10 °C/min).

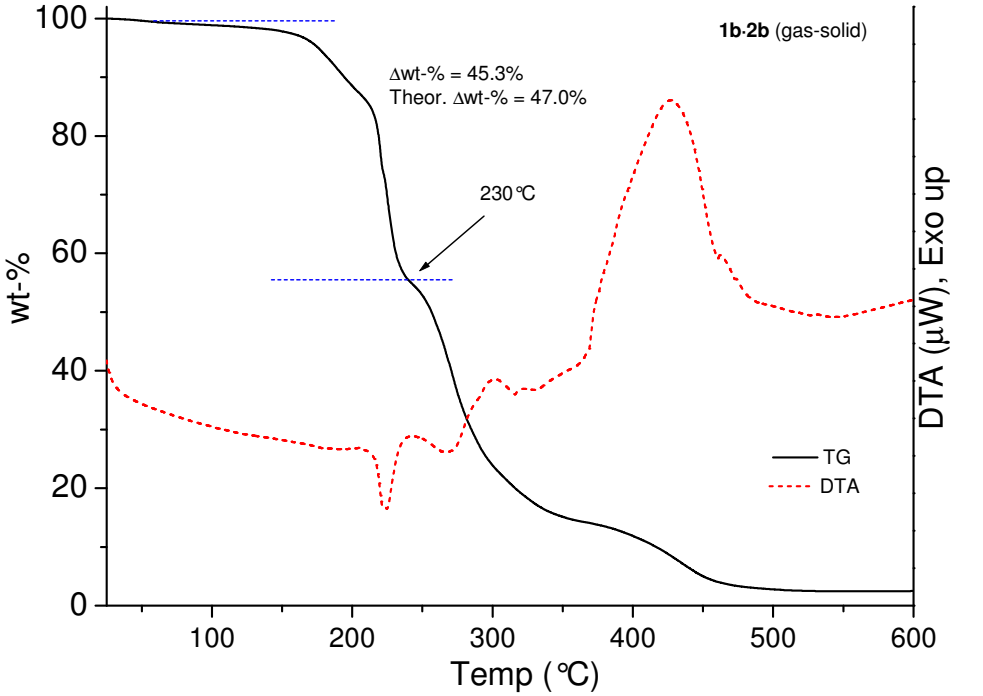

Fig. S23. TG and DTA curves of **1b·2b** obtained from gas-solid reaction (heat rate 10 °C/min).

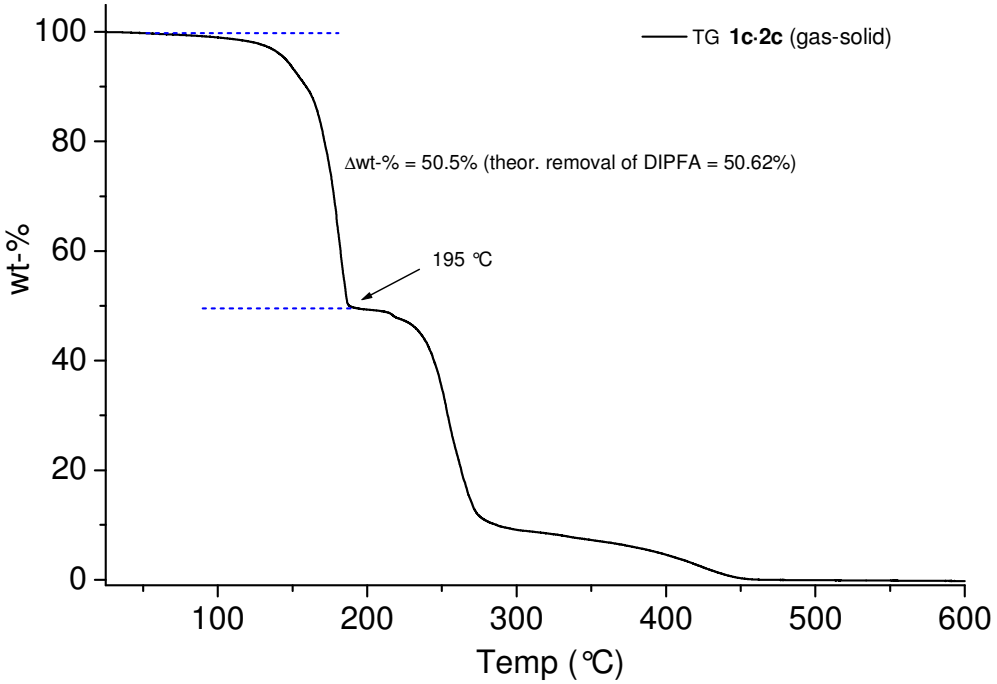

Fig. S24. TG curve of **1c·2c** obtained from gas-solid reaction (heat rate 2 °C/min).

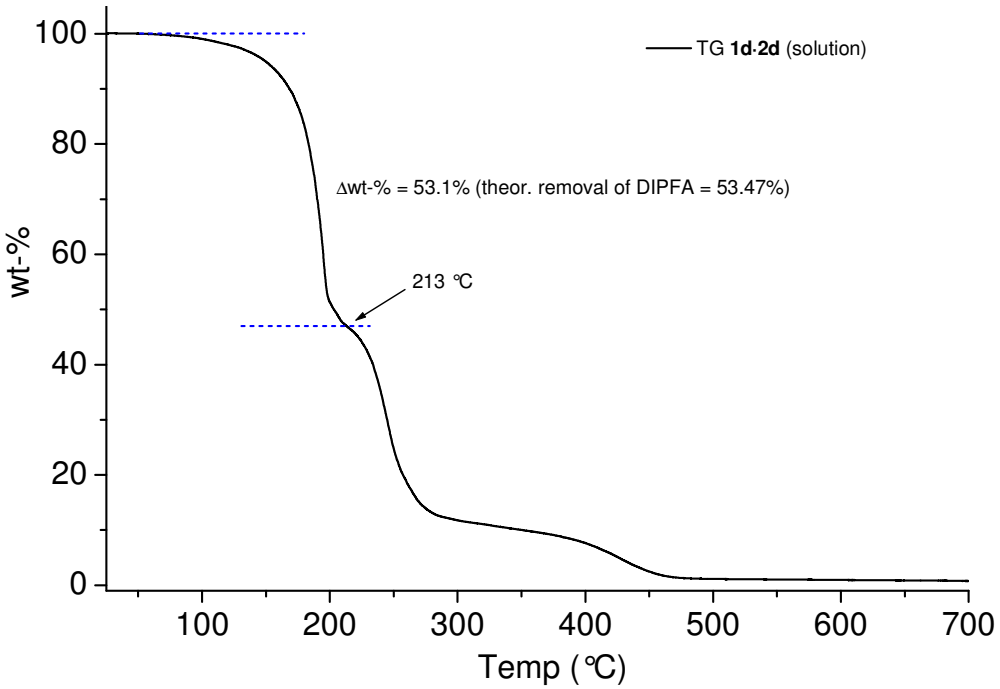

Fig. S25. TG curves of **1d·2d** obtained from solution (heat rate 2 °C/min).

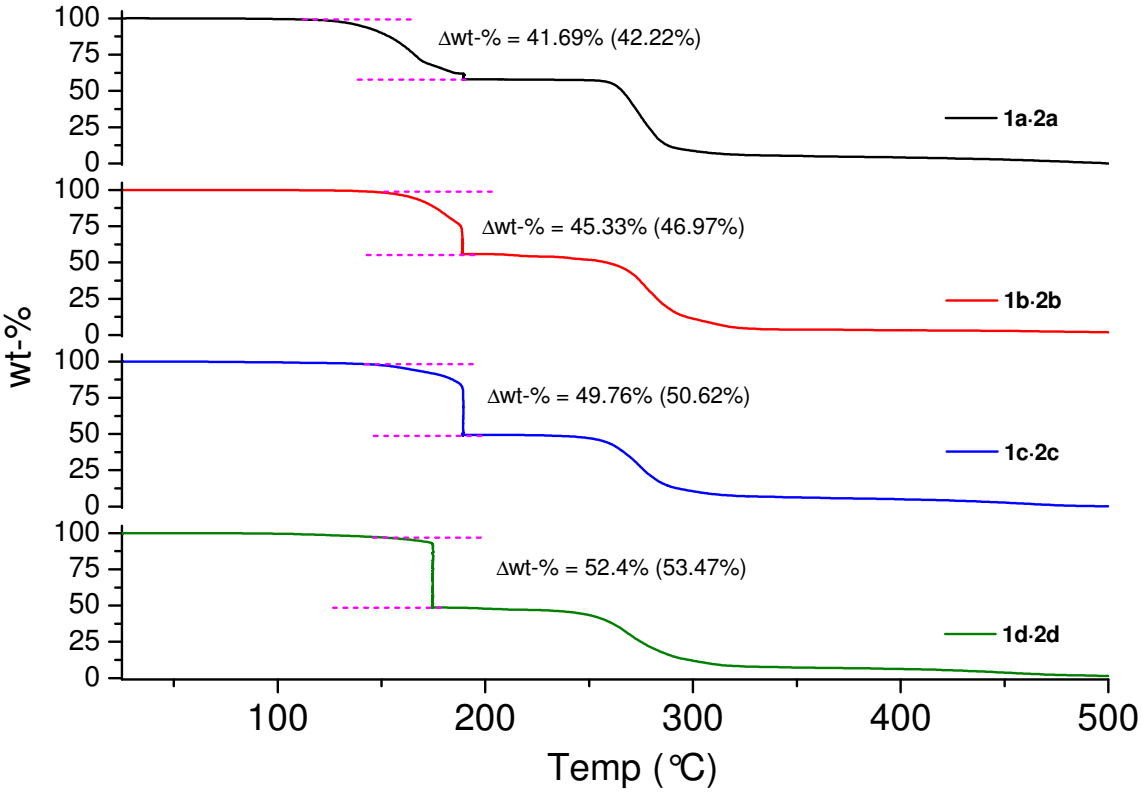

Fig. S26. TG curves of **1a-d·2a-d** obtained from solution (heat rate 10 °C/min with an isothermal step at 190 °C (175 °C on **1d·2d**) for 60 min).

Differential scanning calorimetry

The removal of DIPFAs was clearly demonstrated by the broad endothermic transition which occurred always before the initiation of the melting transition at higher temperature (Figures S27-30 and Table S10). Typically, for example on **1a·2a**, the evaporation of DIPFA starts very slowly above 140°C (see corresponding TG curves), then showing major release of DIPFA between 175-195 °C, and then finally sharp melting transition of the "emptied" complex skeleton can be observed. To enhance separation between transition corresponding to the removal of DIPFA and to final melting of the resulted congener, slower heating rate of 3 °C/min were used also on complexes **1a-c·2a-c** (Fig. S30). Albeit, the slower heating rate was used, the maximum of evaporation transitions are still somewhat at higher temperatures if compared temperatures observed for complete removal of DIPFAs observed on the isothermal TG runs. This is simply due to shorter time period at optimal evaporation temperatures >175 °C, as with used heating rate it takes ~ 10 min to cross the temperature range for example of 175-200 °C compared to 60 min time in case of isothermal TG runs. Finally, the evaporation is more hindered in case of capillary holed DSC pans compared to the fully open platinum pans on TG.

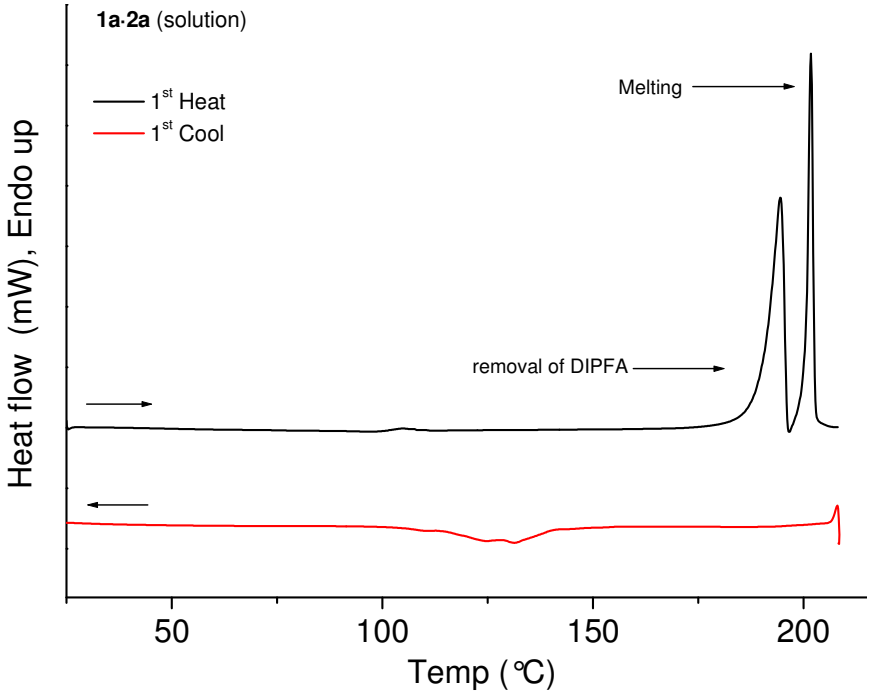

Fig. S27. DSC scans of **1a·2a** obtained from solution (heating rate of 10 °C/min).

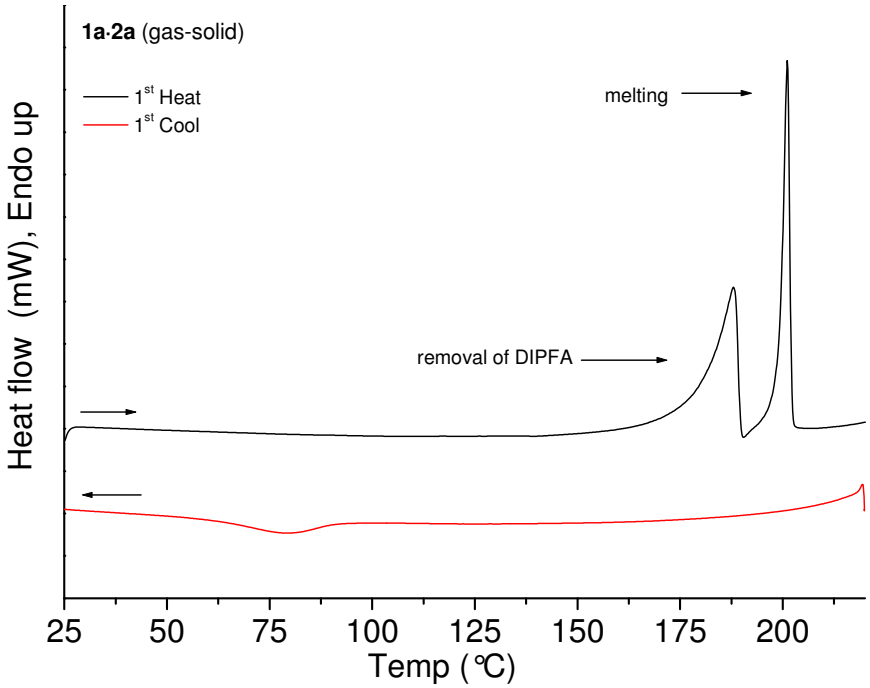

Fig. S28. DSC scans of **1a·2a** obtained from gas-solid reaction (heating rate of 10 °C/min).

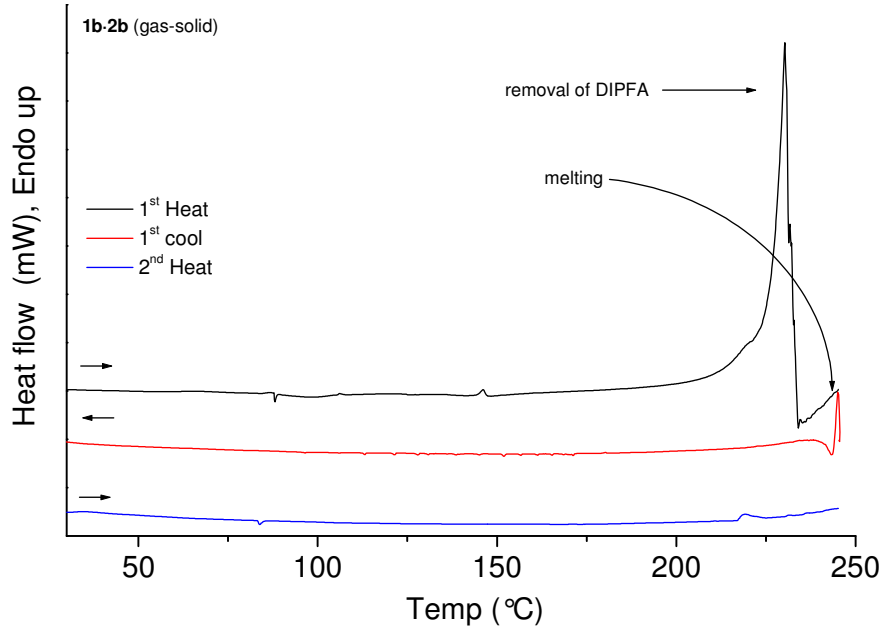

Fig. S29. DSC scans of **1b·2b** obtained from gas-solid reaction (heating rate of 10 °C/min). The 1st heating scan is ended before complete melting of the **1b**, as it starts to decompose on melting.

Table S10. Thermal parameters for complexes **1a-c·2a-c**

Comp.	T_{max} (°C)	T_m (°C)
1a·2a	175-195 *	199-201
1b·2b	210-220 *	238-246 **
1c·2c	211-218 *	218-221 **

T_{max} = peak maximum temperature of evaporation transition, T_m = melting temperature taken as an onset, * = depends on heating rate and ventilation of sample holder, ** = initiation of decomposition on melting complicates defining of the melting onset.

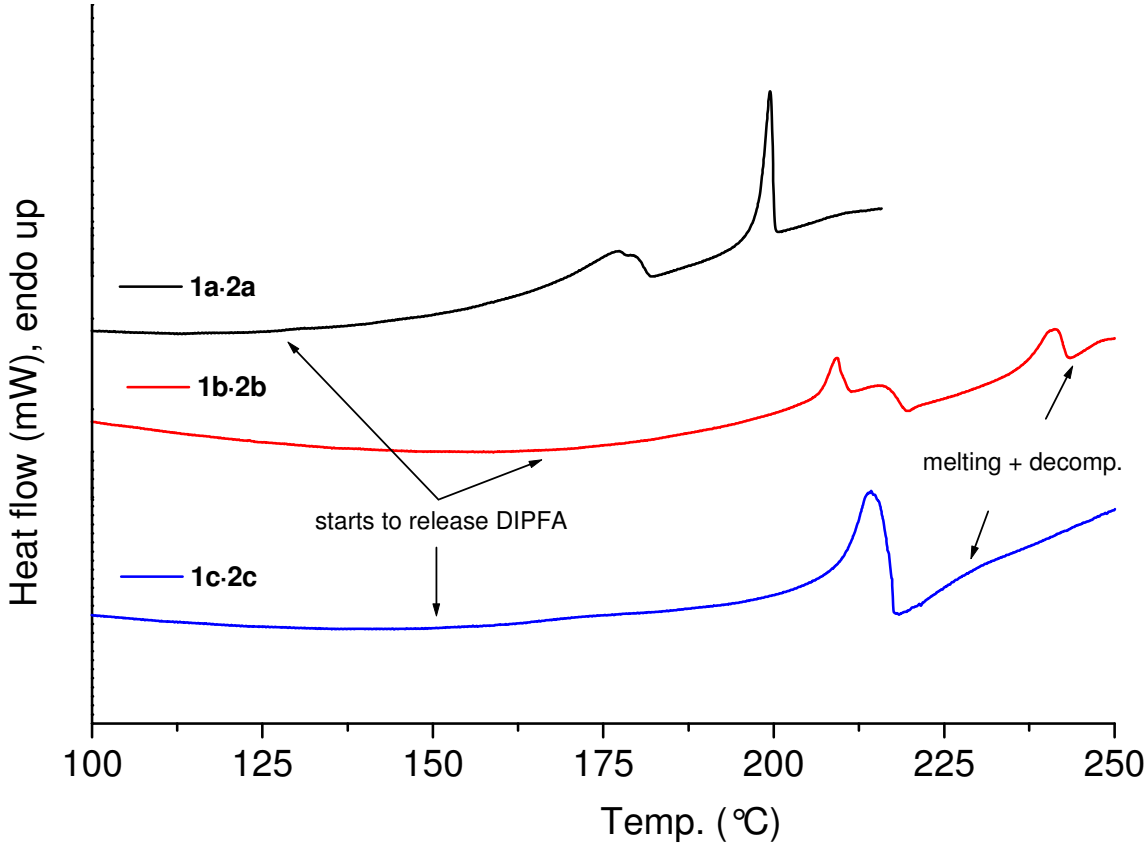

Fig. S30. DSC scans of **1a-c·2a-c** using slow heating rate of 3 °/min.